CAPE PENINSULA
UNIVERSITY OF TECHNOLOGY

Cape Peninsula University of Technology

Faculty of Engineering

Smart Structures and MEMS Lab

Mechanics of Micromachined Bridge-Type Accelerometer

CAPE PENINSULA

UNIVERSITY OF TECHNOLOGY

9000766

Rui Zhang

B.Sc.Eng.(P.R.China)

CPT THE ARC 6213/1 ZH

Submitted towards the Master Degree of Technology
in Mechanical Engineering

Supervisor: **Prof. Dr. Bohua Sun**

Co-Supervisor: **Prof. Dr. Jasson Gryzagoridis**

Cape Town, 2005

Acknowledgments

There are a number of people who sincerely deserve my thanks for their effort in the support of my master's thesis. Firstly, special thanks go to my supervisor Prof. Dr. Bohua Sun who has always been a strong support through all these years of my graduate career and beyond.

I would like to thank my co-supervisor Prof. Dr. Jasson Gryzagoridis and Mr. Keith Jacobs (HOD of Mechanical Engineering) for their kind consideration and help. I would also like to thank all the member of Smart Structures and MEMS Lab for the fantastic environment for friendly atmosphere, and technical support.

I would like to thank Kentron, National Research Foundation (NRF) of South Africa and Cape Peninsula University of Technology (CPUT) for financial support in my research.

Specially, I would like thanks to my parents for their endearing encouragement, patience, and love.

Abstract

Having simple structure and high sensitivity, micro accelerometer is a type of popular transducer used to measure the acceleration in a great variety of conditions. The bridge-type micro accelerometer is a typical micro accelerometer and has many types. As one of research project of Kentron in South Africa, the thesis presented here analyzes the bridge-type capacitive micro accelerometer (BTCMA) and the bridge-type micro accelerometer with two piezoelectric thin films read-out (BTPMA).

In this thesis, the similar structures are used on BTCMA and BTPMA. For proving the fundamental mode of the structure can measure acceleration and utilizing the structural and electric characteristic to avoid the effect of higher modes, the program CoventorWare for micro-electric-mechanical system (MEMS) design and analysis is used here to analyze the modes of these two structures,

The two group piezoelectric thin films of BTPMA can be connected in serial or parallel configurations. Integrating piezoelectric effect method, strength method and energy method, the analytical analysis of these two configurations has been done with particular emphasis on the elastic characteristics of the thin films. The analytical formulas of transducer, sensitivity, resonance frequency, noise, quality factor, minimum detectable signal and maximum detectable range are obtained. According to the comparison results between these two configurations, the charge output in parallel configuration is a little more than that in serial configuration and the sensitivity in serial configuration is much higher than that in parallel configuration. Finally, a calculation of certain practical micro accelerometer size is used to prove the above conclusions.

On the base of capacitance theory, strength method and energy method, the analytical analysis of the BTCMA has been done in this thesis. The analytical formulas of transducer, sensitivity, resonance frequency, noise, quality factor, minimum detectable signal and maximum detectable range are obtained, and these formulas are linearized by using Fourier series theory. After that, a calculation of certain practical micro accelerometer size is used. The program CoventorWare for MEMS design and analysis is used to analyze the structure to obtain the static parameter, dynamic curve, frequency curve and impact of dimension. These results are very closed to the numerical results. To take into account of the mismachining tolerance and stress, Monte Carlo Analysis and Impact of Curvature Analysis are used to perform the influences of mismachining tolerance and stress for structural performance. The results indicate that the influences of mismachining tolerance and stress for structural performance are very limited and the conclusion of analytical analyses can be used on the design of the BTCMA.

Through the analyses in this thesis, the BTCMA has high sensitivity, but its maximum detectable range is much less than that of the BTPMA. So the BTCMA is suitable on high accuracy measurement and BTPMA can be applied into large acceleration and high impulsion measurement.

摘要

微型加速度计具有结构简单、灵敏度高等特点，因此被广泛应用于各种环境下加速度的测量。桥式微加速度计作为典型的微加速度计具有不同的类型。作为南非 Kentron 公司的研究项目之一，本文只对压电和电容两种形式的桥式微加速度计进行分析。

本文中双压电薄膜输出桥式微加速度计（bridge-type micro accelerometer with two piezoelectric thin films read-out）和桥式电容微加速度计（bridge-type capacitive micro accelerometer）采用类似结构。为了检验结构的主振态是否能够测量被测加速度并利用传感器的结构特性和电学特性避免其后续振态对于测量的干扰，文中使用专用 MEMS 设计分析软件 CoventorWare 对这两种结构进行了初步的模态分析。

双压电薄膜输出桥式微加速度计（bridge-type micro accelerometer with two piezoelectric thin films read-out）的两组压电薄膜片可以采用串连和并联两种连接形式，本文结合压电效应理论、强度理论和能量法等理论，对这两种连接形式均进行了解析分析，并在解析分析过程中，考虑了压电薄膜对于整个机构机械特性的影响，得出了传感器方程、灵敏度、结构频率、噪音、质量因子、最小测量精度以及最大测量范围等技术参数的解析公式。经过对这两种连接形式的加速度计性能进行比较，并联结构的输出电荷略多于串连结构的输出电荷，而串连结构的灵敏度远远高于串联结构。最后对某一具体结构尺寸的传感器进行了数值计算用以验证之前的结论。

本文以电容理论、强度理论及能量法等理论为基础，对桥式电容微加速度计（bridge-type capacitive micro accelerometer）进行了解析分析，得出了传感器方程、灵敏度、结构频率、噪音、质量因子、最小测量精度以及最大测量范围等技术参数的解析公式，并应用傅立叶级数对这些公式进行了线性化处理。其后对某一具体结构尺寸的传感器进行了数值计算。同时利用 CoventorWare 软件对

这一结构进行了模拟分析，得到了相应的静态参数、动态曲线、频率曲线以及各个尺寸对于结构频率的影响效果。其分析结果与数值计算结果相比基本相同，进一步验证了解析分析结果的正确性。考虑到生产中的加工误差和加工应力不可避免，本文利用 CoventorWare 分别对于加工误差和加工应力对于结构性能的影响进行了 Monte Carlo 和曲率影响（Impact of Curvature）分析，表明加工误差和加工应力对于结构性能没有显著的影响，在设计过程中可以使用解析分析的结果。

经过本文的分析可以发现，桥式电容微加速度计灵敏度具有更高的灵敏度，但是测量范围远远小于双压电薄膜输出桥式微加速度计。因此，桥式电容微加速度计适用于高精度测量，而双压电薄膜输出桥式微加速度计适用于大加速度、高冲击的测量。

Table of Contents

List of Figures

List of Tables

Chapter 1

Introduction

1.1 Motivation

The demands for new generations of industrial, military, commercial, medical, automotive and aerospace products have been a strong driving force behind the research and development of sensors. This situation has been further stimulated by the intellectual curiosity of humankind. Global competition among the principal industrial nations has also been a parameter in the equation governing the rate of technological progress.

Under the influence of the micromation-current for the product designing, micro-sensors are increasingly and applied in industry. By integrating the knowledge base associated with advanced materials, information technology and integrated circuitry, these three mega-technologies are facilitating the creation of a new generation of micro-electro-mechanical systems (MEMS). This technology has impacted and will bring revolutionary change to our lifestyles in the future.

For high resonant frequency, micro sensor can be applied in many different fields, such as high-resolution positioning, high strike and tiny mass detection.

During the last decade, a large number of investigations have taken place on the micro-sensor field. For instance, Arjun Selvakumar, Farrokh Ayazi and Khalil Najafi (1996) designed a z-axis capacitive accelerometer with large sensitivity. Chingwen. Yeh and Khalil Najafi (1995) created a low-voltage tunneling-based silicon micro accelerometer, which is fabricated using bulk silicon micromaching technology and the boron etch-stop dissolved wafer process. Timo Veijola, Heikki Kuisma and Juha Lahdenpera (1999) researched the possibility of large-displacement capacitive accelerometers. Navid Yazdi, Farrokh Ayazi and Khalil Najafi (1998) presented a

review of silicon micromachined accelerometers. Y. Nemirovsky, A. Nemirovsky, P. Muralt and N. SetterPZT (1996) focused on the design of thin film piezoelectric accelerometer. H.G. Yu, L. Zou, K. Deng, R. Wolf, S. Tadigadapa and S. Trolier-McKinstry (2003) discussed the manufacture of piezoelectric thin film accelerometer. A. Spineanu, P. Benabes and R. Kielbasa (1997) researched the dimensions of piezoelectric thin film accelerometers. D. Eicher, M. Giousouf and W. von Munch (1999) analyzed vibration and electromechanical sensitivity of micro-sensors with four piezoelectric thin films. L. Ries and W. Smith (1999) analyzed various arrangements of deformable sensors using the finite element theory. J. Yu and C. Lan (2001) introduced the design of thin film piezoelectric accelerometer; Qing-Ming Wang, Zhaochun Yang, Fang Li and Patrick Smolinski (2004) performed an analysis on a "+" shape beam with four piezoelectric thin films with particular emphasis on the elastic characteristics of the thin films.

The present work deals with the analysis of a simple structure sensor, bridge-type micro accelerometer. In particular, this thesis focuses on bridge-type micro accelerometer with two piezoelectric thin films read-out and bridge-type capacitive micro accelerometer. The main parameters of these two types of accelerometers are studied. The mode analysis for the models and the numerical simulation of the capacitive accelerometer were obtained using CoventorWare 2004. The results are viewed as design rules for these types of accelerometers.

1.2   Objectives

The major goal of this work was to gain some rules governing the design of the bridge-type micro accelerometers with piezoelectric thin film read-out and bridge-type capacitive micro accelerometer. Supporting tasks, which highlight the major contributions of this thesis, are the following:

- Compare the two connecting configurations of bridge-type micro accelerometer with piezoelectric thin films read-out

- Perform an analysis of bridge-type micro accelerometer with piezoelectric thin films read-out

- Perform an analysis of bridge-type capacitive accelerometers

The ultimate objective is to give guidelines in the design of micro accelerometers, which would assist industry in the manufacture process and product applications.

1.3 Background

1.3.1 Capacitive Accelerometer

Capacitive sensors are generally used for linear rather than angular proximity measurement. Either the dielectric or one of the capacitor plates is movable for angular or linear displacement measurement. Capacitive proximity sensors use the measured object as one plate, while the sensor contains the other plate. The capacitance changes as a function of the area of the plates, the dielectric, or the distance between the plates. Capacitive transducers are available with packaged signal conversion circuitry for DC output operation. Accuracy for small displacements can be near the order of 0.25%, with accuracies of up to 0.05% available at a higher cost. [Hordeski, 1985]

Capacitive acceleration transducers use a change of capacitance in response to acceleration. Some transducer designs use a fixed stator plate and a diaphragm to which a disc shaped seismic mass is attached. The diaphragm acts as the restraining spring as well as the moving electrode of the capacitor. Acceleration acting on the mass causes the diaphragm to deflect and its capacitance to the stator to change proportionally. [Hordeski, 1985]

In the presence of external acceleration, the support frame of an accelerometer moves from its rest position, thus changing the capacitance between the proof mass and a

fixed conductive electrode separated from it with a narrow gap. This capacitance can be measured using electronic circuitry. Silicon capacitive accelerometers have several advantages that make them very attractive for numerous applications ranging from low-cost, large-volume automotive accelerometers [Sherman, 1992], [Ristic, 1993] to high-precision inertial-grade microgravity devices [Rudolf, 1987], [Rudolf, 1990], [Henrion, 1990], [Coulon, 1993], [Warren, 1994], [Yazdi, 1977]. They have high sensitivity, good DC response and noise performance, low drift, low temperature sensitivity, low-power dissipation, and a simple structure.

Some of the most widely used structures for capacitive accelerometers are vertical and lateral structures, as shown in Figure 1.1. Many capacitive accelerometers utilize the vertical structure, where the proof mass is separated by a narrow air gap from a fixed plate, forming a parallel plate sense capacitance [Seidel, 1990], [Peeters, 1992], [Ristic, 1993], [Rudolf, 1987], [Rudolf, 1990], [Henrion, 1990], [Coulon, 1993], [Warren, 1994], [Yazdi, 1977], [Ma, 1994]. In these devices, the proof mass moves in the direction perpendicular to its plane (z-axis) and changes the air gap. In a lateral accelerometer, a number of moving sense fingers are attached to the proof mass, and the sense capacitance is formed between these and the fixed fingers parallel to them.

The sense direction in lateral accelerometers is in the proof-mass plane (x-y directions) [Sherman, 1992], [Boser, 1996], [Chau, 1995], [Drieenhuizen, 1997]. Some designs use a "see-saw" structure, shown in Figure 1.2, where a proof mass is suspended by torsional beams so that one side is heavier than the other side and in response to acceleration in the z-axis, the proof mass moves out of its plane [Cole, 1991], [Spangler, 1995], [Selvakumar, 1996]. The advantages of this structure over conventional parallel-plate z-axis devices are built-in overrange protection, larger sensitivity, and higher pull-in voltage [Selvakumar, 1996].
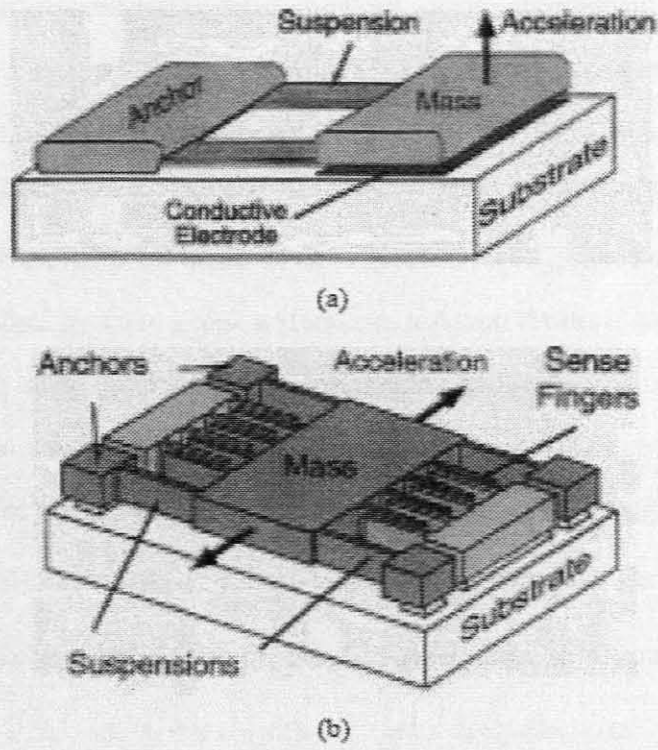
Figure 1.1: Structure of capacitive accelerometers [Selvakumar, 1997].

(a) Vertical

(b) Lateral
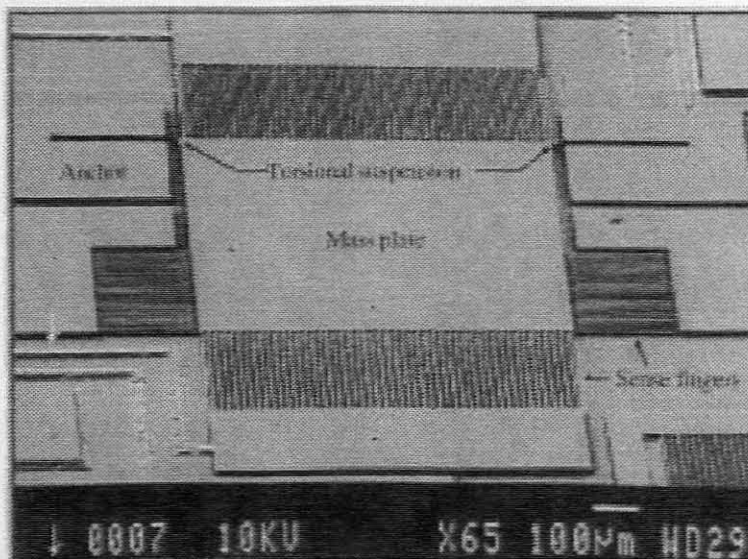
Figure 1.2: A z-axis capacitive torsional accelerometer [Selvakumar, 1996]

The open-loop sensitivity of a capacitive accelerometer is proportional to the proof-mass size and capacitance overlap area and inversely proportional to the spring constant and air gap squared. Early micromachined capacitive accelerometers [Seidel, 1990], [Rudolf, 1987], [Rudolf, 1990], [Henrion, 1990] utilized bulk silicon micromachining and wafer bonding to achieve a thick, large proof mass and high sensitivity. One of the first reported devices [Rudolf, 1987] used a silicon middle wafer anodic bonded to two glass wafers on top and bottom to form a z–axis accelerometer. The device had two differential sense capacitors, with the proof mass forming the middle electrode and metal on the glass wafers forming the top/bottom fixed electrodes. The air gap was formed by recessing the silicon or glass wafers. This device with a proof-mass size of $4.6mgr$ and air gap of $2\mu m$ provided μg -level performance. The second generation of this device [Rudolf, 1990] had a resolution of better than $1\mu g/\sqrt{Hz}$ in a bandwidth of zero frequency to $100Hz$, with a temperature coefficient of offset (TCO) of $30\mu g/^\circ C$ and TCS of $150ppm/^\circ C$. To reduce its temperature sensitivity and long-term drift, the later generation of this device was fabricated using three silicon wafers [Coulon, 1993], [Smith, 1994]. Another significant early design with μg performance was fabricated using glass–silicon bonding and bulk micromachining and utilized a closed-loop $\Sigma\Delta$ readout and control circuit to achieve a $120dB$ dynamic range [Henrion, 1990].

A number of capacitive micro-accelerometers with medium resolution have been fabricated using the bulk silicon dissolved wafer process [Ma, 1994], [Rocksatd, 1995], [Yeh, 1995]. Among these, the device reported in [Rocksatd, 1995] is in high-volume production by Ford. The z-axis accelerometer presented in [Ma, 1994] incorporates damping holes in the proof mass to control damping and uses a second silicon wafer, bonded on top, to provide overrange protection. The torsional accelerometer shown in [Selvakumar, 1996] is fabricated using a three-mask

dissolved wafer process. It uses multiple interdigitated fingers and a varying overlap area method of capacitance change to achieve higher linearity, larger pull-in voltage, and lower damping. The device consists of a $12\mu m$ thick boron-doped silicon inertial mass suspended $7.5\mu m$ above the glass substrate by two narrow, high-aspect-ratio, $12\times3\mu m$ torsion beams. A large number of $300\mu m$ -long capacitive sense fingers are attached to the end of the proof mass and are separated by a $2\mu m$ air gap from fixed fingers anchored to the substrate. The accelerometer provides a sensitivity of $20fF/g$ over a range of $\pm4g$ and a bandwidth of $30Hz$ in atmosphere.

1.3.2   Piezoelectric Accelerometer

Piezoelectric crystal materials differ in their essential characteristics, sensitivity, frequency response, bulk receptivity, and thermal response. Some ceramic elements have been reported to exhibit a zero shift when exposed to an environment that includes high stress and high noise. The upper limit of the operating temperature range is given by the Curie point, of Curie temperature of the material. At this temperature, ceramic elements, which are polarized by exposure to an orienting electric field during cooling after firing, lose their polarization. Curie points vary from $120°C$ for barium titanate to about $570°C$ for lead metaniobate; however, some proprietary ceramics with Curie points above $950°C$ have also been developed. [Norton, 1982]

Of the various possible internal mechanical designs (seismic mass and crystal and their support), the center-mounted and inverted center-mounted compression-type designs and the shear design (in which the piezoelectric crystal is stressed in a shear mode instead of a compression mode) provide minimized case sensitivity, that is, sensitivity to acoustic noise, temperature transients, and strains in the mounting

surface, all acting on the case of the accelerometer. Another important factor in mechanical design is minimization of sensitivity to transverse acceleration (acceleration along axes other than the sensing axis).[Norton, 1982]

The sensing element of a piezoelectric accelerometer consists of two major parts:

- Piezoceramic material
- Seismic mass

One side of the piezoelectric material is connected to a rigid post at the sensor base. The seismic mass is attached to the other side. When the accelerometer is subjected to vibration, a force is generated which acts on the piezoelectric element (compare Figure 1.3). According to Newton's Law this force is equal to the product of the acceleration and the seismic mass. By the piezoelectric effect a charge output proportional to the applied force is generated. Since the seismic mass is constant the charge output signal is proportional to the acceleration of the mass.[Http, a]

$$F = m \cdot a$$

charge sensitivity:

$$Bqa = \frac{q}{a}$$

voltage sensitivity:

$$Bua = \frac{u}{a}$$
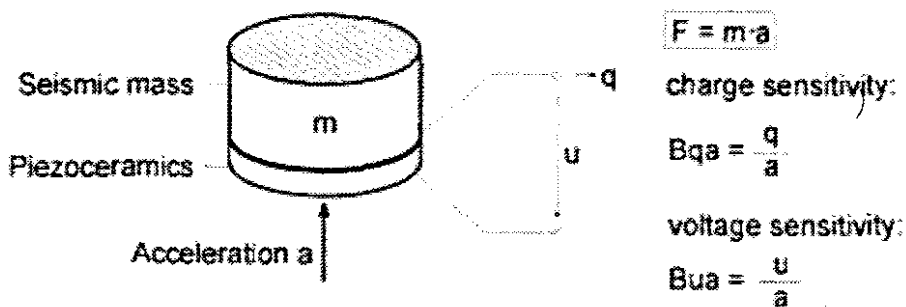
Figure 1.3: Principle of a piezoelectric accelerometer

Over a wide frequency range both sensor base and seismic mass have the same acceleration magnitude. Hence, the sensor measures the acceleration of the test object.

The piezoelectric element is connected to the sensor socket via a pair of electrodes. Some accelerometers feature an integrated electronic circuit which converts the high impedance charge output into a low impedance voltage signal.

The frequency range (over which the frequency response is flat within $\pm 5\%$) of most piezoelectric accelerometers usually has a lower limit between 1 and 3 Hz and an upper limit between 2 and $10\,kHz$ (in a few designs $25\,kHz$ or higher). [Norton, 1982]

A piezoelectric accelerometer can be regarded as a mechanical low-pass with resonance peak. The seismic mass and the piezoceramics (plus other "flexible" components) form a spring mass system. It shows the typical resonance behavior and defines the upper frequency limit of an accelerometer. In order to achieve a wider operating frequency range the resonance frequency should be increased. This is usually done by reducing the seismic mass. However, the lower the seismic mass, the lower the sensitivity. Therefore, an accelerometer with high resonance frequency, for example a shock accelerometer, will be less sensitive whereas a seismic accelerometer with high sensitivity has a low resonance frequency.

The total measurement system capacitance includes the cable capacitance, so a maximum cable length can be used for a maximum frequency and voltage. Source followers can be used for impedance matching: this will solve most of the problems associated with high impedance voltage amplifiers. Calculations for a particular source follower can be used to determine the frequency and output voltage for different values of cable length, or the maximum output voltage and/or frequency for a given cable length. The problem of matching with a follower can be minimized by the use of a charge amplifier system.[Hordeski, 1985]

Jyh-Cheng Yu and Chin-Bing Lan analyzed micro accelerometer consisted of quadri-beam, a seismic mass, and the displacement transducers using piezoelectric

thin films [Yu, 2001]. On the base of them, Qing-Ming Wang, Zhaochun Yang, Fang Li and Patrick Smolinski performed an analysis on a "+" shape beam with four piezoelectric thin films with particular emphasis on the elastic characteristics of the thin films [Wang, 2004]. And continuing their researches, their structure is predigested as a bridge-type accelerometer and using in this work.

1.3.3   Piezoelectric Effect

In 1880, Jacques and Pierre Curie discovered an unusual characteristic of certain crystalline minerals: when subjected to a mechanical force, the crystals became electrically polarized. Tension and compression generated voltages of opposite polarity, and in proportion to the applied force. Subsequently, the converse of this relationship was confirmed: if one of these voltage-generating crystals was exposed to an electric field it lengthened or shortened according to the polarity of the field, and in proportion to the strength of the field. These behaviors were labeled the piezoelectric effect and the inverse piezoelectric effect, respectively, from the Greek word 'piezein', meaning to press or squeeze. [Http, b]

Piezoelectric materials are widely used in actuators, sensors, and similar devices, owing to their ability of changing dimension under an applied voltage and, conversely, generating voltage under applied force.

Figure 1.4 illustrates the behaviors of a PZT cylinder polarized along its axis. For clarity, the magnitude of the effect has been exaggerated.

Figure 1.4(a) shows the cylinder under no-load conditions. If an external force produces compressive or tensile strain in the material, the resulting change in dipole moment causes a voltage to appear between the electrodes. If the cylinder is compressed so that it resumes its original form, i.e. before poling, the voltage will have the same polarity as the poling voltage (Figure 1.4(b)). If it is stretched, the voltage across the electrodes will have opposite polarity to the poling voltage (Figure 1.4(c)).

These are examples of generator action: the conversion of mechanical energy into electrical energy. Examples of piezoelectric induced generator action can be found in cigarette and gas lighters, gramophone pick-ups, accelerometers, hydrophones and microphones.
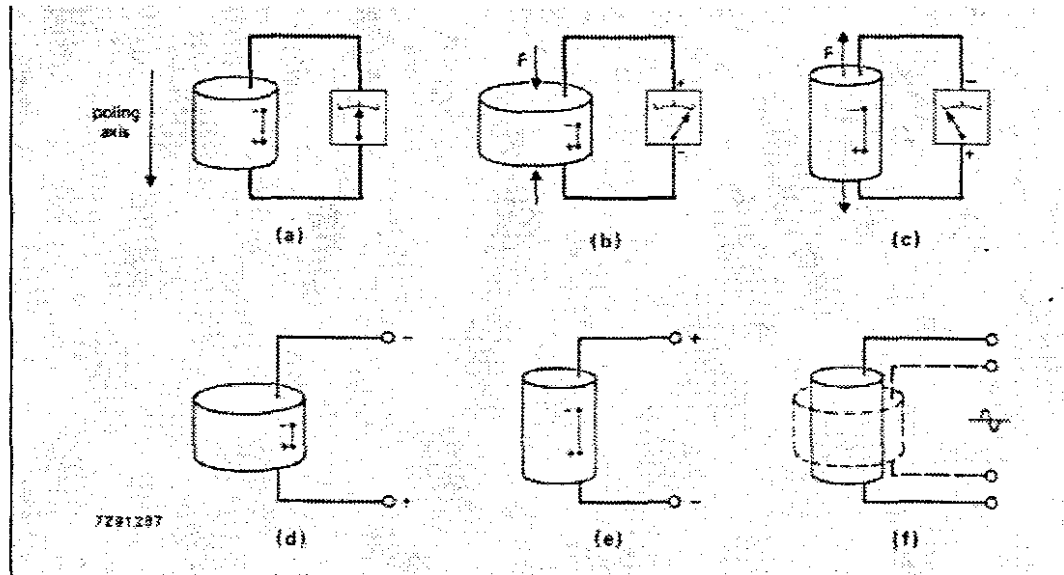
Figure 1.4: The piezoelectric effect in a cylindrical body of piezoelectric ceramic. For the sake of clarity, only a dipole has been drawn in each case.

If a voltage of opposite polarity to the poling voltage in applied to the electrodes, the cylinder will shorten (Figure 1.4(d)). If the applied voltage has the same polarity as the poling voltage, the cylinder will lengthen (Figure 1.4(e)).

Finally, if an alternating voltage is applied to the electrodes, the cylinder will grow and shrink at the same frequency as that of the applied voltage (Figure 1.4(f)). These are examples of motor action: conversion of electrical energy into mechanical energy.

1.3.4 Bandwidth and quality factor, Q, of accelerometers

The bandwidth of an accelerometer refers to its useful range of operating frequencies. This is usually defined by the frequency where the amplitude ratio falls to 0.5, the $3dB$ point. [http, c]

A system's quality factor, Q, describes the sharpness of the system's response. Q is equal to the ratio of the center frequency to the bandwidth. Q is also used to describe the amplitude of the resonant response, which is roughly equal to resonant frequency divided by the driving frequency. [http, c]

1.4 · Scope of Thesis

The organization of this M-tech work is based on the philosophy of vertical technology integration, the predictions of the analytical models and their application to the problem of measuring acceleration.

Chapter 2 details the structures of the capacitive and piezoelectric bridge-type accelerometers, and the mode analysis of these two structures. The purpose of the characterization is two fold: to provide a model for analysis, and to find the fundamental vibration mode that can affect the measuring result. The characterization is divided into two configurations, piezoelectric and capacitive.

Chapter 3 assumes the process of analysis for the two types of accelerometers. The formulations of the main parameters for these two accelerometers are obtained in this chapter. A numerical calculation, applied to a model, is performed.

Chapter 4 presents the results of the model used. A commercially available Finite Element program (CoventorWare 2004) has been employed to model the device. The characters of each device can be laid out vividly.

Chapter 5 closes the thesis with principal conclusions from each chapter.

Chapter 2

Fabrication of Structure and Mode Analysis of Bridge-Type Micro Accelerometers

2.1   Introduction

Before analyzing, the model must be constituted first. This chapter introduces the structures of the two types of accelerometers, and gives the equivalent connection configure of the piezoelectric thin films read-out laid on the suspending beams of the bridge-type micro accelerometer with two piezoelectric thin films read-out.

When the accelerometers are measuring, the devices will be in vibrating condition. The vibration modes will perhaps induce some measuring error. So the mode analysis will be done and the detectable units are composed to avoid the effect of the unneeded modes.

2.2   Structure of Bridge-Type Micro Accelerometer with Two Piezoelectric Thin Films Read-Out

To avoid measuring error in the structure, piezoelectric thin film is built up with two transducer parts and the whole structure will be measured with four piezoelectric transducers (two for each part). As Figure 2.1 shown, the blue parts are the four piezoelectric transducers, the red cube is a seismic mass of the device, and the two yellow parts, which the piezoelectric transducers base on are suspending beams which are fixed at the end.

When acceleration acts on the device, the central seismic mass will vibrate and then the two beams will deform. According to the piezoelectric effect, the piezoelectric thin film will create charge. The voltage will appear between the upper and lower surfaces of the piezoelectric thin film. People can detect this voltage to measure the

acceleration.
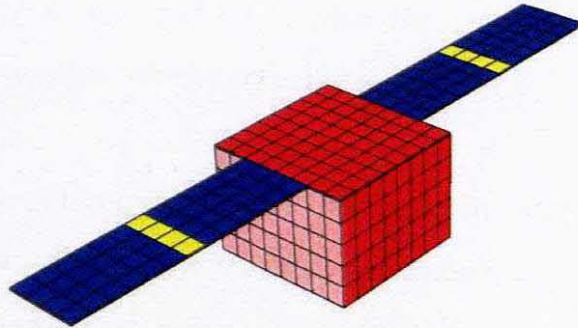
Figure 2.1: 3-D model of the piezoelectric accelerometer

In this structure, the two piezoelectric thin films on the same beam will have opposite polarization. The two piezoelectric thin films on the same beam can be connected in parallel or in series.

(a)   (b)

(c)   (d)
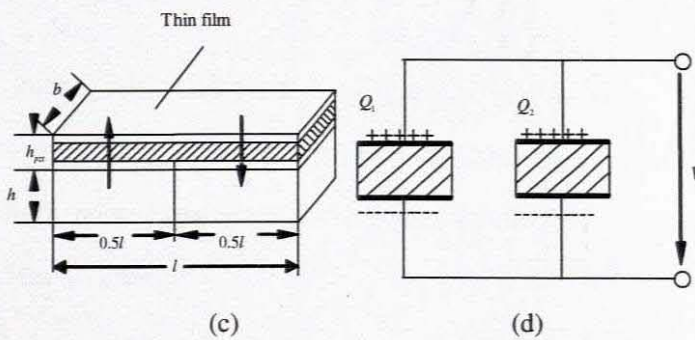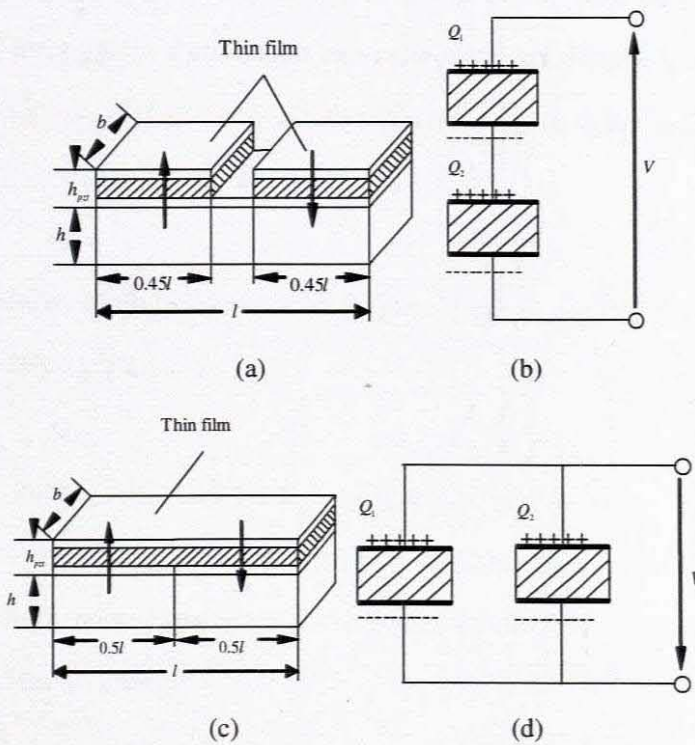
Figure 2.2: The structure and equivalent circuit of series and parallel configuration of

piezoelectric accelerometr

In a series configuration, two piezoelectric thin film transducers connect through lower electrodes and the output terminals are made through the upper electrodes, as shown in Figure 2.2(a). When the two opposite direction stresses caused by the bending of the beam act on each of the two thin films, the two piezoelectric thin films become two power supplies, which connect in series. This is shown in Figure 2.2(b).

In the parallel arrangement, the outputs are made through the upper and lower electrodes of the two piezoelectric thin film transducers, as shown in Figure 2.2(c). Since the stresses of two piezoelectric transducers are in the opposite directions due to the bending of the beam, Figure 2.2(d), the two parallel transducers are like two parallel voltage sources.

2.3   Mode Analysis of Bridge-Type Micro Accelerometer with Two Piezoelectric Thin Films Read-Out

The mode analysis will be done before analyze a device. It can be used to determine the mode that affects the acceleration, and this will be the base mode. Then the output charge created through the base mode can reflect the acceleration along the direction of the base mode. In this project, all the analyses were done using CoventorWare 2004, and the first six modes are shown in Figure 2.3.

As the figures show, in the second mode (Figure 2.3(b)), the two beams dose not bend, so there is no charge generated.

In the fourth (Figure 2.3(d)) and the fifth (Figure 2.3(e)) mode, the two transducers of each beam demonstrate symmetric bending. So the charge produced in the two transducers located on the two parts have equal value and opposite polarity, so the whole structure has no charge.

For the whole structure, the charge output cannot be detected.
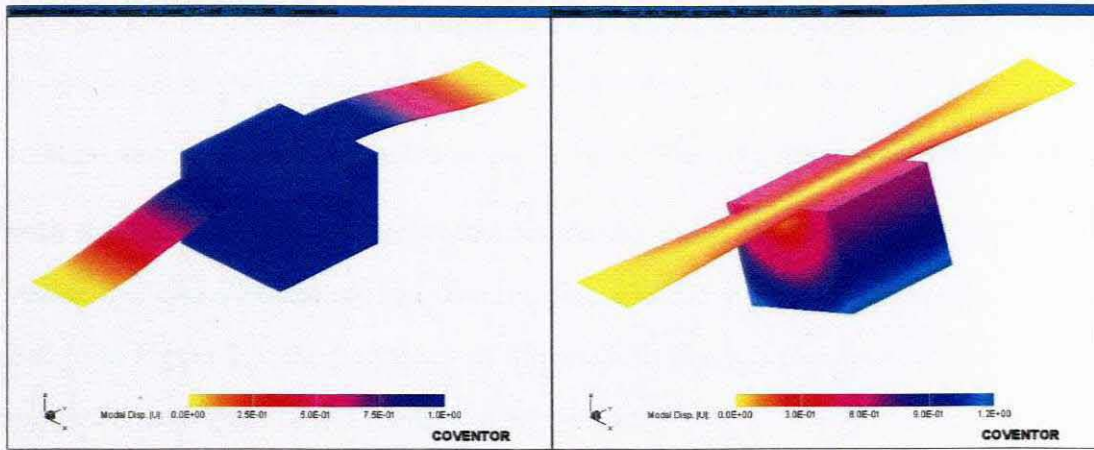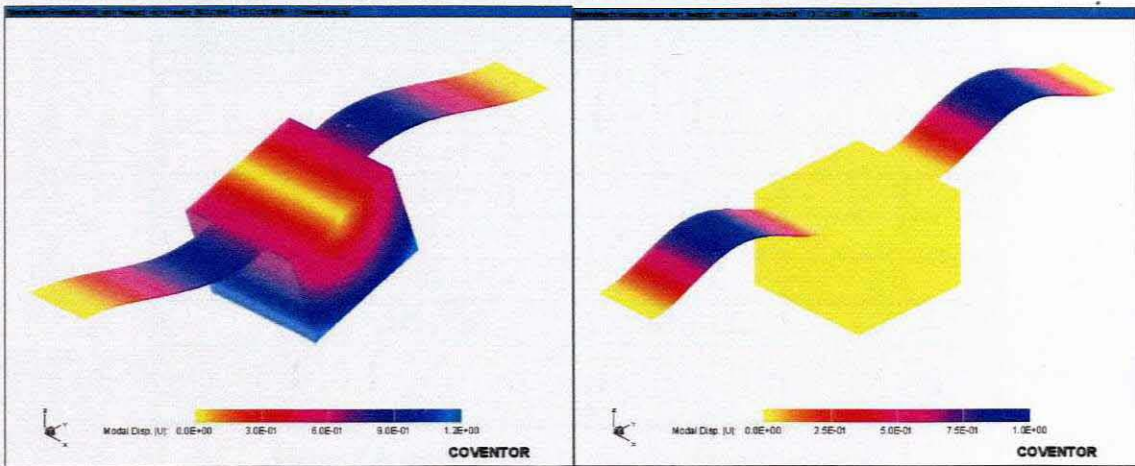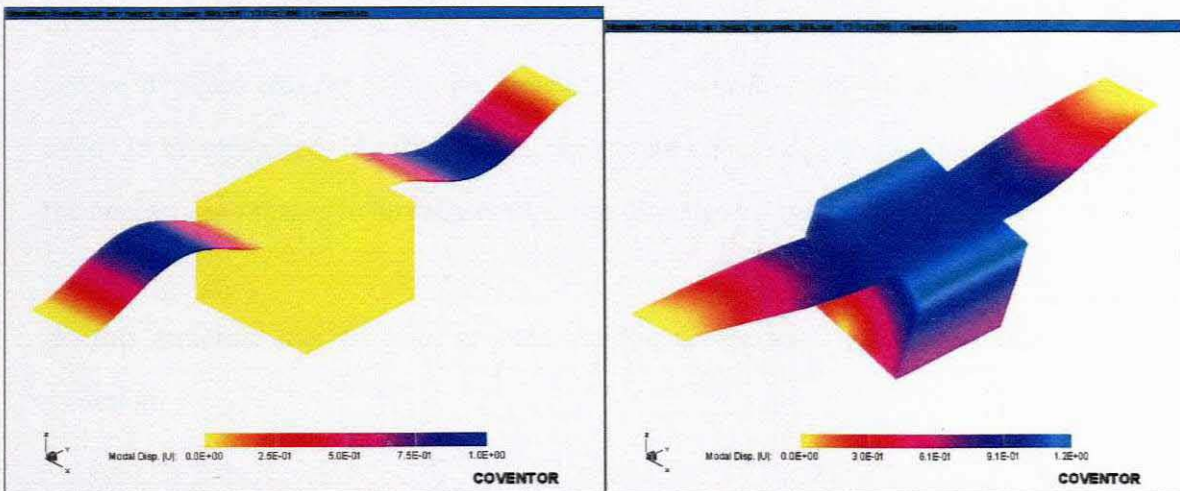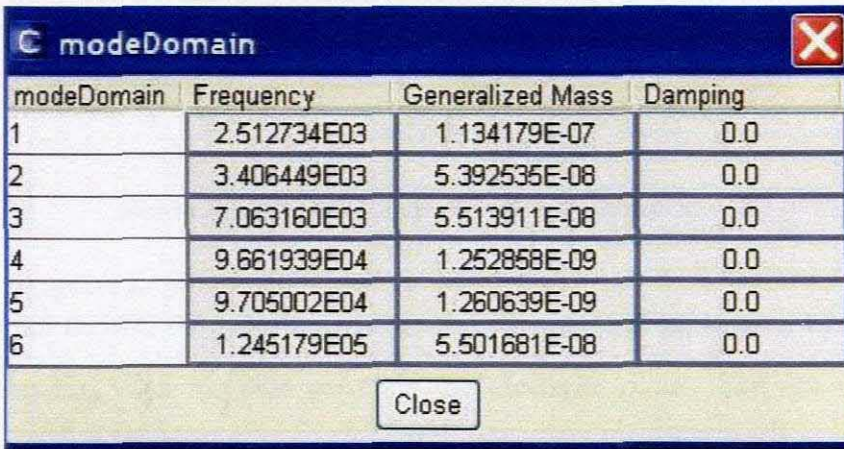
Figure 2.3: The mode caused by piezoelectric acceleration

In the third mode (Figure 2.3(c)), the two beams (transducer parts) have symmetric deformation. So the two beams output the same value, with opposite polarity charges. In the sixth mode (Figure 2.3(f)), the deformation of the model is composed of rotation on y axis and translation on x axis. The rotation on y axis is similar with the second mode, so the beams would not bend. Translation on x axis will course the beams extending, and then the piezoelectric thin film will produce charges. But from Figure 2.4, the frequency of this mode is much higher than the fundamental mode. So the impact of this mode will be ignored.

C modeDomain			
modeDomain	Frequency	Generalized Mass	Damping
1	2.512734E03	1.134179E-07	0.0
2	3.406449E03	5.392535E-08	0.0
3	7.063160E03	5.513911E-08	0.0
4	9.661939E04	1.252858E-09	0.0
5	9.705002E04	1.260639E-09	0.0
6	1.245179E05	5.501681E-08	0.0
	Close		

Figure 2.4: mode analysis of piezoelectric accelerometer

In the first mode (Figure 2.3(a)), which is the base vibration mode, the charge output can be detected and the vibration direction is consistent with the acceleration which needs to be measured. In other words, the output charge of the base mode can reflect the acceleration that is to be measured in the direction of base vibration mode.

So this structure can be used to measure the acceleration quiet accurately in one direction.

2.4   Structure of Bridge-Type Capacitive Micro Accelerometer

In this project, structure of bridge-type capacitive micro accelerometer is similar with bridge-type micro accelerometer with two piezoelectric thin films read-out, which is shown on Figure 2.5.
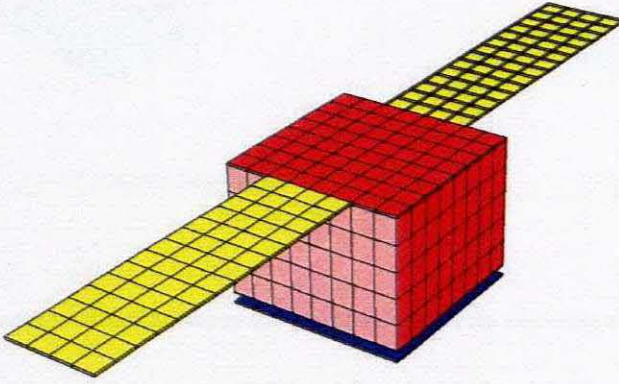
Figure 2.5: 3-D model of the capacitive accelerometer

As Figure 2.5 shown, the yellow parts are the two suspending beams, which will be fixed on the end. And the blue parts are the electrode plates. The red cube is the seismic mass of the device.

In this structure, the area of electrode will be less than the horizontal section area of the seismic mass to avoid the impact of the vibration modes except the fundamental one.

2.5   Mode Analysis of Bridge-Type Capacitive Micro Accelerometer

Because the structures of two micro accelerometers are similar, the vibration modes are also similar (shown as Figure 2.6). But the impact of each mode will not be same.

As the figures show, in the fourth (Figure 2.6(d)) and the fifth (Figure 2.3(e)) mode, the seismic mass does not move. It means that the gap between the seismic mass and the electrode does not change. So the capacitance between them will not change. In other word, there is no effect to the measurement.

(a)

(b)

(c)

(d)

(e)

(f)
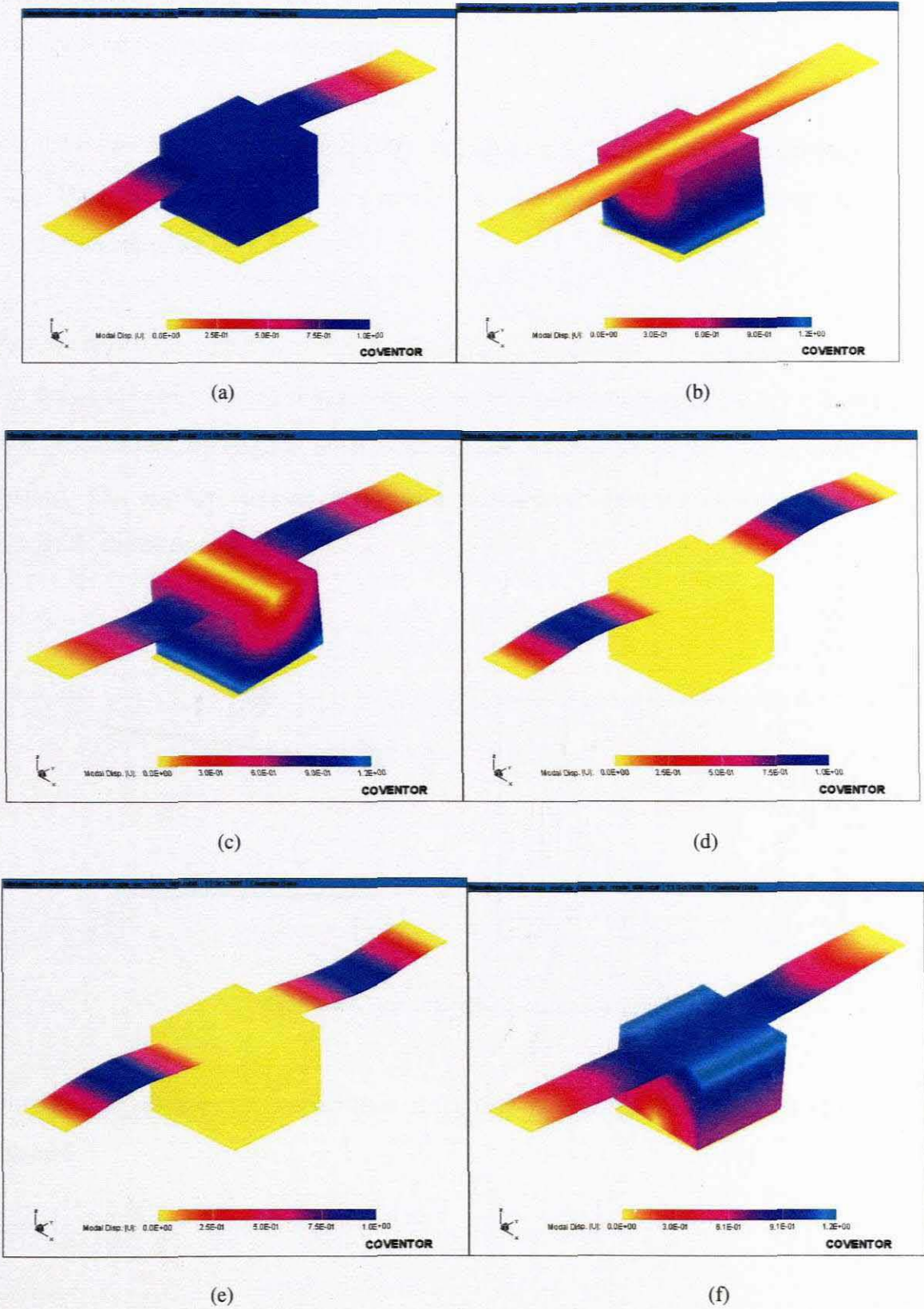
Figure 2.6: The mode caused by capacitive acceleration

In the second mode (Figure 2.6(b) and the third mode (Figure 2.6(c)), the seismic mass is rotated along the y-axis and x-axis. Then the seismic mass and the electrode will constitute a tilted-plate capacitor.

For these two modes, the movable plate will rotate a tiny angle along the symmetry axis. Then the two plates are not parallel, so the two plates will compose to a tilted-plate capacitor.

First we derive the equation of tiny angle tilted–plate capacitor C in general. Figure 2.7 shows the structure and dimensions of the tiny angle tilted-plate capacitor, build xOz coordinate, the original point is located in the middle of the bottom plate's surface. The average distance of the two plates is d, and the effective area is $S = a \times b$, the tilted angle is θ.
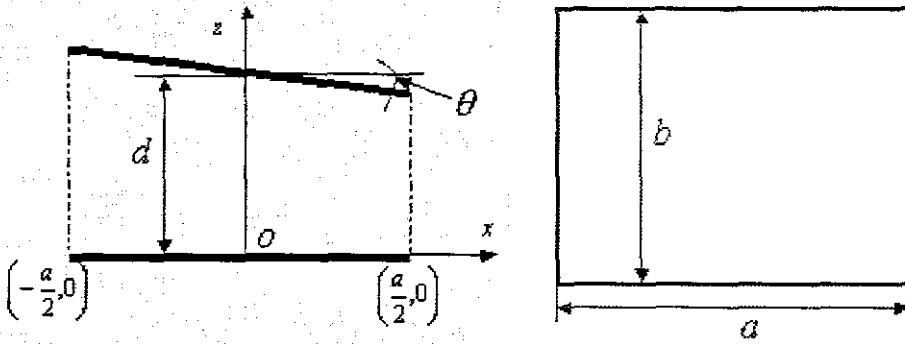
Figure 2.7: Tiny angle tilted –plate capacitor

Through integral, the exact capacitance of the tiny angle tilted-plate capacitor can be obtained:

$$C = \varepsilon \int_{-\frac{a}{2}}^{\frac{a}{2}} \frac{bdx}{tg\theta x + d} \tag{2.1}$$

To tiny angle tilted-plate capacitor, θ is very small, so the capacitance can be

approximated following:

$$tg\theta \approx \theta$$

Then, Eq.(2.1) will predigest to:

$$C = \varepsilon \int_{-\frac{a}{2}}^{\frac{a}{2}} \frac{bdx}{\theta x + d} \tag{2.2}$$

In Eq.(2.2), the denominator can be transformed as:

$$\frac{1}{\theta x + d} = \frac{d - \theta x}{(d - \theta x)(d + \theta x)} = \frac{d - \theta x}{d^2 - \theta^2 x^2} \tag{2.3}$$

When θ is a tiny angle:

$$\theta^2 \approx 0 \tag{2.4}$$

Substituting Eq.(2.4) into (2.3), there will be:

$$\frac{1}{\theta x + d} = \frac{d - \theta x}{d^2} \tag{2.5}$$

Substituting (2.5) into (2.2), the capacitance will be:

$$C = \frac{\varepsilon}{d^2} \int_{-\frac{a}{2}}^{\frac{a}{2}} b(d - \theta x)dx = \frac{\varepsilon ba}{d} = \varepsilon \frac{S}{d} \tag{2.6}$$
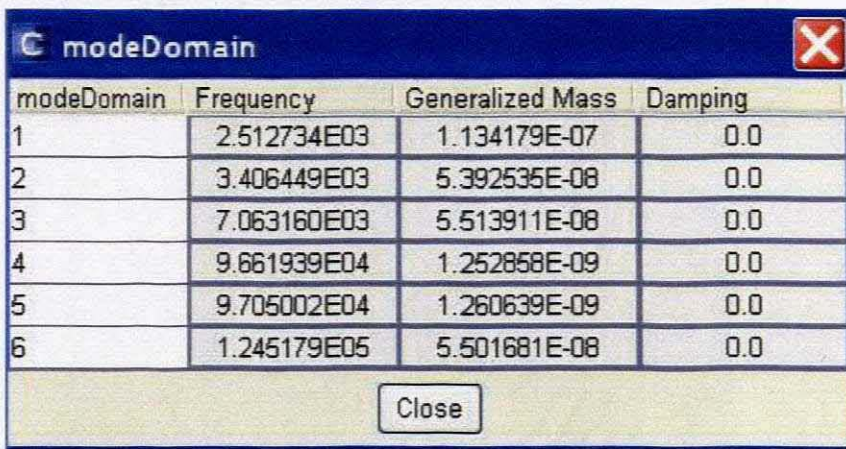
Thereby, for the tiny angle tilted-plate capacitor, the value of its capacitance is the dielectric constant multiply by area divide by the average distance between the two plates.

In the second and third modes, the average distance equals to the initial distance between the two electrode plates. For these two modes, if the area of fixed plate is smaller than that of the moveable plate, the effective area will not change. Integrating above, the capacitance in these two modes will not change.

In the sixth mode (Figure 2.6(f)), the deformation of the model is composed of a rotation on y axis and translation on x axis. The rotation on y axis is similar with the second mode so the rotation will be ignored. Because we design the area of the electrode is smaller than the horizontal section area of the mass, the translation will not cause any change of the capacitance.

In the first mode (Figure 2.6(a)), which is the base vibration mode, the charge output can be detected and the vibration direction is consistent with the acceleration which needs to be measured. In other words, the output charge of the base mode can reflect the acceleration that is to be measured in the direction of base vibration mode.

So this structure can be used to measure the acceleration quiet accurately in one direction.

modeDomain	Frequency	Generalized Mass	Damping
1	2.512734E03	1.134179E-07	0.0
2	3.406449E03	5.392535E-08	0.0
3	7.063160E03	5.513911E-08	0.0
4	9.661939E04	1.252858E-09	0.0
5	9.705002E04	1.260639E-09	0.0
6	1.245179E05	5.501681E-08	0.0

Figure 2.8: mode analysis of capacitive accelerometer

Figure 2.8 gives us the frequency analysis of each mode. We can discover the frequency of the fundamental mode (natural frequency) is different with Figure 2.4. From Figure 2.1, the accelerometer has four piezoelectric transducers base on the two suspending beams. Then the elastic coefficient will become lager and the natural frequency will be lager.

2.6   Summary

According to the analysis above, the possible effects of the unneeded mode to the measurement have been eliminated. The devices can be used to detect the acceleration on a single direction and can get an exact result. The idiographic analytical calculation and analysis on software will be in the following two chapters.

Chapter 3
Analysis of Bridge-Type Micro Accelerometers with Two Piezoelectric Thin Films Read-Out

3.1   Introduction

The most important effort of this work is that has studied the properties of the bridge-type micro accelerometer with two piezoelectric thin films read-out The desired outcome of analytical modeling is to obtain predictions of the properties response of the bridge-type micro accelerometer with two piezoelectric thin films read-out products. These effective properties then become a way to describe the averaged response of the bridge-type micro accelerometer with two piezoelectric thin films read-out for applications.

Model used in this chapter has been introduced and mode analysis has been done in Chapter 2. Generally, for a group of transducer, there should be two configures of connection. The two different connecting configures will cause different properties, and the different types of micro accelerometers with same structure will also cause different properties. In this chapter, firstly, based on the piezoelectric effect method and strength method, the analysis of two connecting configures will be done. After that, the formula of the properties can be obtained. The micro accelerometer can be designed and optimized with analogous structure.

The journal paper [Sun, 2004] for the analysis of the bridge-type micro accelerometer with two piezoelectric thin films read-out with piezoelectric thin films has been published on Journal of Ningbo University. On the base of this chapter, the analysis for piezoelectric pressure sensor has been written to a conference paper [Sun, 2005] and joined NSTI Nanotech 2005.

3.2   Assumption

Based on the mode analysis, the first mode of the structure will be used to determine the acceleration. The following assumptions are made in the model of this section:

1) Compared with the central seismic mass, the mass of the beams and piezoelectric thin films are too small they can be ignored;

2) The central seismic mass and rim of the whole structure are rigid;

3) piezoelectric thin films and beams are elastic and they obey Hooke's law;

4) The material of piezoelectric transducer is orthotropic;

5) With the central seismic mass only subjected to vertical acceleration and pure bending deformation originated in the beams, the strains in 2-direction and the stress in the 3-direction can be ignored compared with the other strains and stresses. The directions are defined as Figure 3.1.
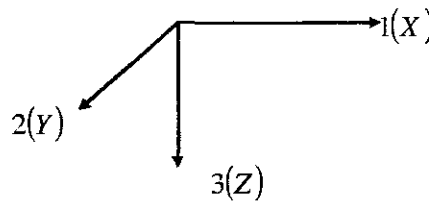
Figure 3.1: Direction of the coordination

3.3   Formula of Accelerometer

Using the two piezoelectric thin films read-out structure, there are two cases: series and parallel configurations. The structure has the two beams fixed on each end, and each beam's performance is shown in Figure 3.2.
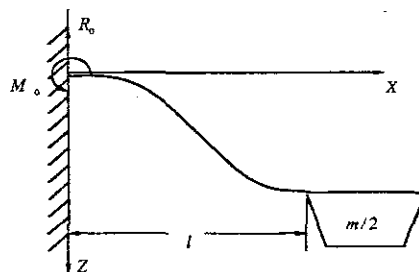
Figure 3.2: The deformation of the suspending beam

According to assumption 5:

$$\sigma_3 = \sigma_5 = \sigma_6 = 0 \tag{3.1}$$

and

$$\varepsilon_2 = \varepsilon_4 = \varepsilon_6 = 0 \tag{3.2}$$

Commonly the strains in each direction are always expressed with the following symbols:

$$\begin{pmatrix} \sigma_1 & \sigma_2 & \sigma_3 & \sigma_4 & \sigma_5 & \sigma_6 \end{pmatrix}^T = \begin{pmatrix} \sigma_{xx} & \sigma_{yy} & \sigma_{zz} & \sigma_{yx} & \sigma_{x} & \sigma_{xy} \end{pmatrix}^T$$

When the acceleration is induced on the seismic central mass, the reaction force induces a deflection on the suspending beam. Because of this, it follows that the force equilibrium along three directions should be given by the following reaction force:

$$R_0 = \frac{1}{2} m \ddot{z} \tag{3.3}$$

Where m is central mass.

From the boundary conditions, we have the moment:

$$M(x) = \frac{1}{2} m \ddot{z} \left(\frac{l}{2} - x \right) \tag{3.4}$$

Where l is the length of the beam.
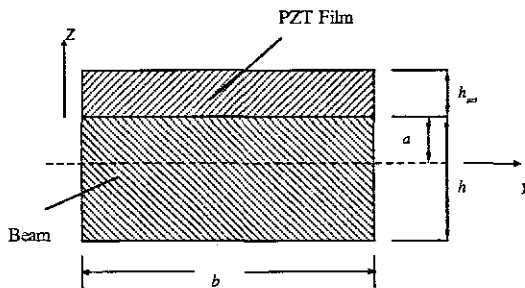
Figure 3.3: Corss-section of the suspending beam

Figure 3.3 is a cross-section of the beam. Assuming good boundary strains between the piezoelectric thin films and the beam, in other words a perfect bond between the two, the strain can be given by:

$$\varepsilon_1 = \frac{z}{\rho} \tag{3.5}$$

Where ρ is the radius of bending.

From constitutive equations and based on assumption 4, the stress of the piezoelectric thin film is defined as follow:

$$\sigma_3 = C_{31}\varepsilon_1 + C_{32}\varepsilon_2 + C_{33}\varepsilon_3 \tag{3.6}$$

Substituting Eqs.(3.1) and (3.2) into Eq.(3.6), we have:

$$\varepsilon_3 = -\frac{C_{31}}{C_{33}}\varepsilon_1 \tag{3.7}$$

Therefore, the stress of the piezoelectric thin film σ_1 can be written as:

$$\sigma_1 = \left(C_{11} - \frac{C_{31}C_{13}}{C_{33}} \right)\varepsilon_1$$

If

$$E_P = C_{11} - \frac{C_{31}C_{13}}{C_{33}}$$

then

$$\sigma_1 = E_p \varepsilon_1 \tag{3.8}$$

We consider the material of the beam to be anisotropic, then the stress on beam $\bar{\sigma}_1$ can be written as:

$$\overline{\sigma}_1 = \frac{E_2}{1-\mu^2}\overline{\varepsilon}_1$$

Where $\overline{\varepsilon}_1$ is the strain on the beam, E_2 is Young's Modulus, and μ is Poisson's ratio of the beam.

We define:

$$E_B = \frac{E_2}{1-\mu^2}$$

then

$$\overline{\sigma}_1 = E_B\overline{\varepsilon}_1 \tag{3.9}$$

For the cross-section shown in Figure 3.3, we have the following result from force equilibrium in one-direction:

$$\int \sigma dA = \int E\frac{z}{\rho}bdz = 0$$

$$\int \sigma z dA = \int E\frac{z}{\rho}zbdz = M(x)$$

or

$$\int_{-(h-a)}^{a} bE_B\frac{z}{\rho}dz + \int_{a}^{h_{pz}+a} bE_P\frac{z}{\rho}dz = 0 \tag{3.10}$$

$$\int_{-(h-a)}^{a} bE_B\frac{z}{\rho}zdz + \int_{a}^{h_{pz}+a} bE_P\frac{z}{\rho}zdz = M(x) \tag{3.11}$$

Where a is the distance to the neutral axis of the beam measured from the interface, b is the width of the beam, h is the thickness of the beam, h_{pz} is the thickness of the piezoelectric thin film, and $M(x)$ is the moment on the cross-section.

From Eq.(3.10):

$$a = \frac{h^2 E_B - h_{pzt}^2 E_P}{2hE_B + 2h_{pzt}E_P} \qquad (3.12)$$

From Eq.(3.11):

$$\rho M(x) = \frac{1}{3}\left[bE_B\left(h^3 - 3h^2 a + 3ha^2\right)\right] + \frac{1}{3}\left[bE_P\left(h_{pzt}^3 + 3h_{pzt}^2 a + 3h_{pzt}a^2\right)\right]$$

or

$$\rho M(x) = EI_{eq} \qquad (3.13)$$

Substituting Eqs.(3.5), (3.12), and (3.13) into Eq.(8), the average stress in the piezoelectric thin film can be found:

$$\sigma_1 = E_P \varepsilon_1 = \frac{E_P}{EI_{eq}}\left(\frac{h_{pzt}}{2} + a\right)m\ddot{z} \qquad (3.14)$$

Assuming all the stresses are caused by bending, the contribution from any infinitesimal portion to the total charge is shown as follow:

$$D_3 = d_{31}\sigma_1 \qquad (3.15)$$

Where d_{31} is the piezoelectric coefficient.

Substituting Eq.(3.14) into the integration of Eq.(3.15), we can find the total charge output of piezoelectric thin film over one suspending beam in a series and in a parallel condition.

In a series connection the acceleration formula is:

$$Q_S = \int_0^{0.45l} D_{31}bdx - \int_{0.55l}^{l} D_{31}bdx$$
$$= 0.12375d_{31}b\frac{E_P}{EI_{eq}}\left(\frac{h_{pzt}}{2} + a\right)l^2 m\ddot{z} \qquad (3.16)$$

In a parallel connection the acceleration formula is:

$$Q_P = 2\int_0^{0.5} D_{31} b \, dx$$

$$= 0.125 d_{31} b \frac{E_P}{EI_{eq}} \left(\frac{h_{pzt}}{2} + a \right) l^2 m \ddot{z}$$

(3.17)

From Eqs.(3.16) and (3.17), we can see that there is a linear relationship between the acceleration $\ddot{z}$ and the total charge Q, and the formulas include piezoelectric coefficient d_{31}, elastic coefficient E_P, thickness h for the thin film, and length l and elastic coefficient E_B for the beam. So we can adjust any of these parameters to increase or decrease the charge output. The aim of this work is to increase the output. ·

3.4   Sensitivity Analysis

The sensitivity is defined as the ratio of the open-circuit voltage and acceleration:

$$S_V = \frac{V}{\ddot{z}} = \frac{Q}{\ddot{z}C}$$

(3.18)

Then the sensitivity in each condition can be obtained:

In a series structure:

$$S_V^S = \frac{Q_S}{\ddot{z}C_S} = 0.12375 d_{31} b \frac{E_P}{EI_{eq}} \left(\frac{h_{pzt}}{2} + a \right) \frac{l^2 m}{C_S} \cdot$$

(3.19)

and in a parallel structure:

$$S_V^P = \frac{Q_P}{\ddot{z}C_P} = 0.125 d_{31} b \frac{E_P}{EI_{eq}} \left(\frac{h_{pzt}}{2} + a \right) \frac{l^2 m}{C_P}$$

(3.20)

From the formulas above, sensitivity is the voltage produced by one unit of voltage reflected on the piezoelectric thin film. The sensitivity is a direct ratio with the total charge output and inverse ratio with the capacitance of piezoelectric thin film. Similar to the acceleration formulas, the sensitivity formulas include piezoelectric coefficient d_{31}, thickness h, elastic coefficient E_P of piezoelectric thin film, and length l and

elastic coefficient E_B of the suspending beam. So, we can adjust some of these to increase the sensitivity.

3.5 Total Charge Output and Sensitivity Comparison

To determine the best connection mode, we need to compare the total charge output and sensitivity of these two structures.

3.5.1 Total charge output comparison

$$\frac{Q_P - Q_S}{Q_S} \times 100\% = \frac{0.125 - 0.12375}{0.12375} \times 100\% = 1.01\%$$

The total charge output in parallel structure is larger than in series structure by about 1%.

3.5.2 Sensitivity comparison

$$\frac{S_V^S}{S_V^P} = \frac{0.12375 d_{31} b \dfrac{E_P}{EI_{eq}} \left(\dfrac{h_{pzt}}{2} + a \right) \dfrac{l^2 m}{C_S}}{0.125 d_{31} b \dfrac{E_P}{EI_{eq}} \left(\dfrac{h_{pzt}}{2} + a \right) \dfrac{l^2 m}{C_P}}$$

$$= \frac{0.12375 C_P}{0.125 C_S}$$

$$= 0.99 \times \frac{2 \dfrac{\varepsilon_r \varepsilon_0 b l_{PZT}^P}{h_{PZT}}}{\dfrac{\varepsilon_r \varepsilon_0 b l_{PZT}^S}{2 h_{PZT}}}$$

$$= 0.99 \times \frac{4 l_{PZT}^P}{l_{PZT}^S}$$

$$= 0.99 \times 4 \times \frac{0.5l}{0.45l} = 0.99 \times 4 \times 1.11 = 4.4$$

Where C_1 and C_2 are the capacitances of the two piezoelectric transducers.

The sensitivity in series connection mode is larger than in parallel.

3.6   Natural Frequency Analysis

The accelerometer is an inertia system. So we can transform the device to an equivalent mass-spring inertia system. This device follows the elastic formula:

$$F = kx \tag{3.21}$$

The reaction force is shown in Eq.(3.3). From the boundary conditions, the real bending moment will be:

$$M = M_0 - \frac{1}{2}Fx \tag{3.22}$$

Where M_0 is assumptive bending moment.

From Figure 3.2, when the displacement up to max, the rotation angle of the end $(x = l)$ which is connected with concentrative mass θ_l is still 0 $(\theta_l = 0)$ since the mass will never bend. (δ is the max displacement)

In terms of the particularity of this structure (two sides fixed), we use the theorem of energy--*Castigliano's Theorem* to require the max displacement of the beam in succession.

The denotation of strain energy is U.

$$U = \int_0^l \frac{M^2}{2EI_{eq}} dx \tag{3.23}$$

Apply $\theta_0 = 0$ to require bending moment

$$\theta_0 = \frac{\partial U}{\partial M_0} = \int_0^l \frac{M}{EI_{eq}} \frac{\partial M}{\partial M_0} dx = \frac{1}{EI_{eq}} \int_0^l \left(M_0 - \frac{1}{2}Fx \right) dx = 0 \tag{3.24}$$

By solving this equation, the bending moment is:

$$M_0 = \frac{1}{4} Fl \tag{3.25}$$

Then the max displacement will be:

$$\delta = \frac{\partial U}{\partial F_B} \int_0^l \frac{M}{EI_{eq}} \frac{\partial M}{\partial F_B} dx = \frac{F}{2EI_{eq}} \int_0^l \left(\frac{l}{2} - x\right)^2 dx = \frac{Fl^3}{24EI_{eq}} \tag{3.26}$$

In Eq.(3.21), we consider $x = \Delta \delta$, then Eq.(3.26) can transform to:

$$x = \frac{Fl^3}{24EI_{eq}} \tag{3.27}$$

Then

$$k = \frac{F}{x} = \frac{24EI_{eq}}{l^3} \tag{3.28}$$

To inertia system, the natural frequency can calculate as:

$$f = \frac{1}{2\pi} \sqrt{\frac{k}{m}} \tag{3.29}$$

Substituting Eq.(3.28) into Eq.(3.29), the formula will become to:

$$f = \frac{1}{2\pi} \sqrt{\frac{2EI_{eq}}{ml^3}} \tag{3.30}$$

3.7 Noise Analysis

There are many contributors to noise in an accelerometer. MEMS sensors are so small that the Brownian noise of the devices must be considered, while it is usually ignored in larger sensors. In micromechanical systems, the sensor noise floor is often set by the thermo-mechanical noise. This noise arises from the thermal motion of the atoms inside the structure and in the air (Brownian motion).

The Brownian noise equivalent acceleration of the system is [Gabrielson, 1993]:

$$a_e = \frac{\sqrt{4k_B T D}}{m}$$ (3.31)

Where k_B is Boltzmann's constant ($k_B = 1.38 \times 10^{-23} J/K$), T is absolutely temperature ($T = 300K$), and D is damping coefficient.

The exact value of the damping coefficient D does not need to be computed and can be dominated with the quality factor, Q, of the system under harmonic excitation according the following formula:

$$D = \frac{\sqrt{km}}{Q}$$ (3.32)

Where is k - the elastic coefficient of the system, m is the general mass.

And we can get the value of the quality factor through the following formula:

$$Q = \frac{d\sqrt{mk}}{\mu_0 A}$$ (3.33)

Where d is the gap between the mass and the substrate, A is the area of horizontal cross-section of the mass, and μ_0 is the viscosity of air at 27°C ($\mu_0 = 18 \times 10^{-6} kg/m \cdot s$)

Substituting Eqs.(3.32) and (3.33) into Eq.(3.31), we have

$$a_e = \sqrt{\frac{4\mu_0 k_B T A}{dm^2}}$$ (3.34)

3.8   Minimum Detectable Signal

The minimum detectable signal (MDS) is a very useful parameter for the sensors. From the analyses above, we can get the thermal noise equivalent voltage spectral density as follow [Connor, 1982]:

$$N_0 = a_e S_V \qquad\qquad (3.35)$$

The bandwidth of the system is:

$$BW = \frac{\sqrt{k/m}}{Q} \qquad\qquad (3.36)$$

Then the minimum detectable signal will be obtained:

$$MDS = \frac{N_0 \times \sqrt{BW}}{S_V}$$
$$= \frac{\sqrt{4k_B TDBW}}{m} \qquad\qquad (3.37)$$
$$= \frac{\mu_0 A}{d} \times \sqrt{\frac{4k_B T}{m^3}}$$

From Eq.(3.37), we can see that whatever the configuration is, the minimum detectable signals are same.

3.9 Dynamic Analysis

Because the mode in this paper is simulated with the mode used in [Wang, 2004], the result of dynamic analysis is also simulated.
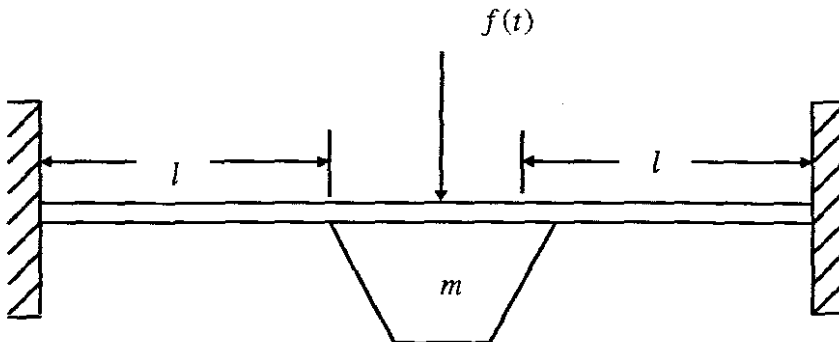
Figure 3.4: Dynamic model of the accelerometer

The dynamic model is subjected to a periodic force $f(t)$, as shown schematically by

Figure 3.4. The sinusoidal force can be written as:

$$f(t) = mg \sin 2\pi f t \tag{3.38}$$

Where $g = 9.8 m/s^2$, and f - the driving frequency.

Causing only the first vibration mode is considered, the general solution of the beam is given by [McCallion, 1973]

$$z(x) = a_1 \cos(\beta x) + a_2 \sin(\beta x) + a_3 \cosh(\beta x) + a_4 \sinh(\beta x) \tag{3.39}$$

In which, a_1, a_2, a_3, a_4, β are constants.

From the boundary conditions, the first normal mode of the micro accelerometer can be obtained as

$$z_1(x) = V_a[\sin kx - \sinh(kx) + S(\cos kx - \cosh(kx))]$$
$$= V_a g(x)$$

Where $k = 4.73/2l$.

$$S = \frac{(\sinh(kl) - \sin kl)}{(\cos kl - \cosh(kl))} \tag{3.40}$$

and V_a is constant.

Since the first normal is orthogonal, V_a can be obtained by

$$\int_0^{2l} \gamma(x) A(x) z_1^2(x) dx = 1 \tag{3.41}$$

Where $\gamma(x)$ is the density, and A is the cross-sectional area.

Assuming that the seismic mass is much larger that the mass of the beam, the above equation can then be simplified

$$V_a = \sqrt{\frac{g^2(l)}{m}} \tag{3.42}$$

From Rayleigh method, the fundamental natural frequency f_n is given by

$$f_n^2 = 2\int_0^l \frac{dU_{max}}{4\pi^2 K_{e\,max}}$$
(3.43)

Where $K_{e\,max} = mz_1^2(l)$

For beam with single elastic layer, we have

$$dU_{max} = \frac{1}{2}\left(\frac{d^2 z_1}{dx^2}\right)^2 EI$$
(3.44)

Using the expansion theorem, the displacement of the micro accelerometer is

$$z(x,t) = z_1(x)\eta(t)$$
(3.45)

$\eta(t)$ is the modal coordinate given by

$$\eta(t) = \frac{1}{2\pi f_n}\left(\int_0^t N(\tau)\sin(2\pi f_n)(t-\tau)d\tau\right)$$
(3.46)

And N is the modal force given by

$$N(t) = \int_0^{2l} z_1(x)f(x,t)dx$$
(3.47)

Substituting Eqs.(3.38), (3.45) and (3.46) into Eq.(3.44), we have

$$z(x,t) = \frac{V_a^2 mgz(l)[\sin 2\pi f t - (f/f_n)\sin 2\pi f_n t]}{(2\pi f_n)^2 - (2\pi f)^2}$$
$$\times[\sin kx - \sinh(kx) + S(\cos kx - \cosh(kx))]$$
(3.48)

So

$$\frac{1}{\rho} = \frac{d^2 z}{dx^2}$$
(3.49)

Therefore, the average stresses at the cross-sectional area of piezoelectric film σ_1 can be obtained by Eq.(3.14). The charger output of piezoelectric films can then be calculate by Eqs.(3.16) and (3.17):

$$Q_S = \frac{d_{31}bE_P\left(\dfrac{h_{PZT}}{2}+a\right)\times V_a^2 mg\ddot{z}(l)\left[\sin 2\pi ft - \left(\dfrac{f}{f_n}\right)\sin 2\pi f_n t\right]}{(2\pi f_n)^2 - (2\pi f)^2}$$
$$\times [T(0.45l) - T(0) - T(l) + T(0.55l)] \tag{3.50}$$

and

$$Q_S = \frac{d_{31}bE_P\left(\dfrac{h_{PZT}}{2}+a\right)\times V_a^2 mg\ddot{z}(l)\left[\sin 2\pi ft - \left(\dfrac{f}{f_n}\right)\sin 2\pi f_n t\right]}{(2\pi f_n)^2 - (2\pi f)^2}$$
$$\times [T(0.5l) - T(0)] \tag{3.51}$$

Where $T(x) = k[-S\sinh(kx) - S\sin kx + \cos kx - \cosh(kx)]$.

Using Eqs.(3.50) and (3.51), the charger output of the device under dynamic excitation can be predicted.

3.10 Stress Analysis

Eq.(3.4) shows the maximum of moment is at $x = 0$. We assume there is only vertical acceleration applied to the central seismic mass, then the piezoelectric film and silicon layer are primarily subjected to stresses in the one-direction, and the other stresses are too small and can be ignored. Therefore, the maximum stress can be obtained either at the upper surface or at the lower surface.

At the upper surface:

$$\sigma_{max1} = \frac{E_P m\ddot{z}l(h_{pzt} + a)}{4EI_{eq}} \tag{3.52}$$

And at the lower surface:

$$\sigma_{max\,2} = \frac{E_B m \ddot{z} l(h-a)}{4EI_{eq}} \tag{3.53}$$

Therefore, σ_{max} can be obtained by selecting the larger one of $\sigma_{max\,1}$ and $\sigma_{max\,2}$.

Then the maximum detectable range can be calculated by:

$$\ddot{z}_{max} = \frac{4\sigma_b EI_{eq}}{E_m mltg} \tag{3.54}$$

Where causing the thickness of silicon layer is much larger than piezoelectric film, σ_b is intensity limit of silicon. When $\sigma_{max\,1} > \sigma_{max\,2}$, $E_m = E_P$ and $t = h_{pz} + a$. Otherwise, $E_m = E_B$ and $t = h - a$.

3.11   Numerical Calculation

To gain an intuitionistic result, the parameters of the micro accelerometers can be calculated according the above formulas. The geometry of the structure used for our modeling is given in Table 3.1. And the mechanical properties of the materials are shown as Table 3.2. In Table 3.2, the C-matrix is as following:

$$\left[C^E\right] = \begin{bmatrix} 12.03 & 7.52 & 7.51 & 0 & 0 & 0 \\ 7.52 & 12.03 & 7.51 & 0 & 0 & 0 \\ 7.51 & 7.51 & 11.09 & 0 & 0 & 0 \\ 0 & 0 & 0 & 2.11 & 0 & 0 \\ 0 & 0 & 0 & 0 & 2.11 & 0 \\ 0 & 0 & 0 & 0 & 0 & 2.26 \end{bmatrix} \times 10^{10} \left(N/m^2\right)$$

Table 3.1: Dimension of accelerometer

Length of suspension beam, l (μm)	700
Width of suspension beam, b (μm)	200
Thickness of suspension beam, h (μm)	5
Gap between the mass and substrate, d (μm)	20
Length of seismic mass, l_m (μm)	400
Width of seismic mass, b_m (μm)	400
Thickness of seismic mass, h_m (μm)	300
Thickness of piezoelectric thin film, h_{PZT} (μm)	0.5

Table 3.2: Mechanical properties of materials

	Silicon	piezoelectric
Young's modulus (N/m^2)	1.9×10^{11}	C - matrix
Poisson's ratio	0.18	
Density (kg/m^3)	2330	7750
Fracture strength (N/m^2)	7×10^9 [Peterson, 1982]	
Dielectric constant ($K_3 = \varepsilon_{33}/\varepsilon_0$) ($\varepsilon_0 = 8.85 \times 10^{-12}$)	730	1700
Piezoelectric coefficient, d_{31} ($\times 10^{-12} C/N$)		-171

The seismic mass will be:

$$m = V_m \rho$$
$$= l_m b_m h_m \rho$$
$$= 400 \times 10^{-6} \times 400 \times 10^{-6} \times 300 \times 10^{-6} \times 2330$$
$$= 1.1184 \times 10^{-7} kg$$

Substituting the dimension and the material properties of the device, we can calculate:

$$E_P = C_{11} - \frac{C_{31}C_{13}}{C_{33}}$$
$$= 12.03 - \frac{7.51 \times 7.51}{11.09}$$
$$= 6.944$$

$$E_B = \frac{E_2}{1-\mu^2}$$

$$= \frac{1.9 \times 10^{11}}{1-0.18^2}$$

$$= 1.9636 \times 10^{11}$$

$$a = \frac{h^2 E_B - h_{pzt}^2 E_P}{2hE_B + 2h_{pzt}E_P}$$

$$= \frac{\left(5 \times 10^{-6}\right)^2 \times 2.23 \times 10^{11} - \left(0.5 \times 10^{-6}\right)^2 \times 6.944}{2 \times 5 \times 10^{-6} \times 2.23 \times 10^{11} + 2 \times 0.5 \times 10^{-6} \times 6.944}$$

$$= 2.4999999999992 \times 10^{-6}$$

From Eq.(3.13):

$$EI_{eq} = \frac{1}{3}\left[bE_B\left(h^3 - 3h^2 a + 3ha^2\right)\right] + \frac{1}{3}\left[bE_P\left(h_{pzt}^3 + 3h_{pzt}^2 a + 3h_{pzt}a^2\right)\right]$$

$$= \frac{1}{3}\left[\begin{array}{l} 200 \times 10^{-6} \times 2.23 \times 10^{11} \\ \times \left(\begin{array}{l} \left(5 \times 10^{-6}\right)^3 - 3 \times \left(5 \times 10^{-6}\right)^2 \times 2.4999999999992 \times 10^{-6} \\ + 3 \times 5 \times 10^{-6} \times \left(2.4999999999992 \times 10^{-6}\right)^2 \end{array} \right) \end{array} \right]$$

$$+ \frac{1}{3}\left[\begin{array}{l} 200 \times 10^{-6} \times 6.994 \\ \times \left(\begin{array}{l} \left(0.5 \times 10^{-6}\right)^3 - 3 \times \left(0.5 \times 10^{-6}\right)^2 \times 2.4999999999992 \times 10^{-6} \\ + 3 \times 0.5 \times 10^{-6} \times \left(2.4999999999992 \times 10^{-6}\right)^2 \end{array} \right) \end{array} \right]$$

$$= 4.0909 \times 10^{-10}$$

From Eq.(3.28), the equivalent elastic coefficient will be:

$$k = \frac{24EI_{eq}}{l^3}$$

$$= \frac{24 \times 4.0909 \times 10^{-10}}{\left(700 \times 10^{-6}\right)^3}$$

$$= 28.6244 N/m$$

Then the quality factor, bandwidth, and natural frequency of the system can be obtained:

$$Q = \frac{d\sqrt{mk}}{\mu_0 A}$$

$$= \frac{d\sqrt{km}}{\mu_0 l_m b_m}$$

$$= \frac{20 \times 10^{-6} \times \sqrt{1.1184 \times 10^{-7} \times 28.6244}}{18 \times 10^{-6} \times 400 \times 10^{-6} \times 400 \times 10^{-6}}$$

$$= 1.2425 \times 10^4$$

$$BW = \frac{\sqrt{k/m}}{Q}$$

$$= \frac{\sqrt{\dfrac{28.6244}{1.1184 \times 10^{-7}}}}{1.2425 \times 10^4}$$

$$= 1.2876 Hz$$

$$f = \frac{1}{2\pi}\sqrt{\frac{k}{m}}$$

$$= \frac{1}{2\pi}\sqrt{\frac{28.6244}{1.1184 \times 10^{-7}}}$$

$$= 2.5461 kHz$$

Through Eqs.(3.16) and (3.17), the acceleration formula can be calculated:

$$Q_S = 0.12375 d_{31} b \frac{E_P}{EI_{eq}}\left(\frac{h_{pzt}}{2} + a\right) l^2 m\ddot{z}$$

$$= 0.12375 \times (-171) \times 10^{-12} \times 200 \times 10^{-6} \times \frac{6.9443}{4.0909 \times 10^{-10}}$$

$$\times \left(\frac{0.5 \times 10^{-6}}{2} + 2.4999999999992 \times 10^{-6}\right) \times \left(700 \times 10^{-6}\right)\ddot{z}$$

$$= -1.0827 \times 10^{-23}\ddot{z}$$

(3.55)

$$Q_P = 0.125d_{31}b\frac{E_P}{EI_{eq}}\left(\frac{h_{pzt}}{2}+a\right)l^2 m\ddot{z}$$

$$= 0.125\times(-171)\times10^{-12}\times200\times10^{-6}\times\frac{6.9443}{4.0909\times10^{-10}}$$

$$\times\left(\frac{0.5\times10^{-6}}{2}+2.4999999999992\times10^{-6}\right)\times\left(700\times10^{-6}\right)\ddot{z} \tag{3.56}$$

$$= -1.0936\times10^{-23}\ddot{z}$$

So

$$\ddot{z}_S = -9.236\times10^{22}Q_S(g) \tag{3.57}$$

$$\ddot{z}_P = -9.144\times10^{22}Q_P(g) \tag{3.58}$$

Here, the minus mean the acceleration direction of system is opposite with the movement direction of general mass.

And from Eqs.(3.19) and (3.20), we can get the sensitivity of two configurations:

$$S_V^S = \frac{Q_S}{\ddot{z}C_S}$$

$$= \frac{Q_S}{\ddot{z}\dfrac{\varepsilon_r\varepsilon_0 bl_{PZT}^S}{2h_{PZT}}}$$

$$= \frac{-1.0827\times10^{-23}\times\ddot{z}}{\ddot{z}\times\dfrac{1700\times8.85\times10^{-12}\times200\times10^{-6}\times315\times10^{-6}}{2\times0.5\times10^{-6}}}$$

$$= 1.1423\times10^{-14}V/(g)$$

and

$$S_V^P = \frac{Q_P}{\ddot{z} C_P}$$

$$= \frac{Q_P}{\ddot{z} \dfrac{2\varepsilon_r \varepsilon_0 b l_{PZT}^P}{h_{PZT}}}$$

$$= \frac{-1.0936 \times 10^{-23} \times \ddot{z}}{\ddot{z} \times \dfrac{2 \times 1700 \times 8.85 \times 10^{-12} \times 200 \times 10^{-6} \times 350 \times 10^{-6}}{0.5 \times 10^{-6}}}$$

$$= 2.596 \times 10^{-15} V / (g)$$

From Eqs.(3.31), (3.37), the Brownian noise equivalent acceleration and MDS can be obtained:

$$a_e = \frac{\sqrt{4 k_B T D}}{m}$$

$$= \frac{\sqrt{4 k_B T \dfrac{\sqrt{km}}{Q}}}{m}$$

$$= \frac{\sqrt{4 \times 1.38 \times 10^{-23} \times 300 \times \dfrac{\sqrt{28.6244 \times 1.1184 \times 10^{-7}}}{1.2425 \times 10^4}}}{1.1184 \times 10^{-7}}$$

$$= 4.4554 \times 10^{-8} (g) / \sqrt{Hz}$$

$$MDS = \frac{\mu_0 A}{d} \times \sqrt{\frac{4 k_B T}{m^3}}$$

$$= \frac{\mu_0 l_m b_m}{d} \times \sqrt{\frac{4 k_B T}{m^3}}$$

$$= \frac{18 \times 10^{-6} \times 400 \times 10^{-6} \times 400 \times 10^{-6}}{20 \times 10^{-6}} \times \sqrt{\frac{4 \times 1.38 \times 10^{-23} \times 300}{(1.1184 \times 10^{-7})^3}}$$

$$= 5.0556 \times 10^{-8} (g)$$

From Eq.(3.54), the maximum detectable range can be calculated:

$$\ddot{z}_{max} = \frac{4\sigma_b EI_{eq}}{E_m mlt}$$

$$= \frac{4\sigma_b EI_{eq}}{E_B ml(h-a)}$$

$$= \frac{4 \times 7 \times 10^9 \times 4.0909 \times 10^{-10}}{1.9636 \times 10^{11} \times 1.1184 \times 10^{-7} \times 700 \times 10^{-6} \times \left(5 \times 10^{-6} - 2.4999999999992 \times 10^{-6}\right)}$$

$$= 3.0413 \times 10^4 (g)$$

From this result, the proposed micro accelerometer can be used to detect a large acceleration.

In Table 3.3, we have shown the nonlinear relationship between acceleration coefficient, sensitivity and length of beam l.

3.12 Summary

In this chapter, the analyses for two configure of the bridge-type micro accelerometer with two piezoelectric thin films read-out have been done. The main characteristics of the bridge-type micro accelerometer with two piezoelectric thin films read-out have been calculated and given as formulation. All the properties of the imaginary model have been calculated according to these formulas. People can get an intuitionistic impression from it.

Table 3.3: Nonlinear relationship between parameters and length of beam l

	Formula	Diagram
Quality Factor	$Q = 1.2425 \times 10^4$	
Resonance Frequency	$f = 2.5461 kHz$	
Bandwidth	$BW = 1.2876 Hz$	
Acceleration Coefficient in the series configuration	$Q_S / \ddot{z} = -2.21 \times 10^{-5} l^2$	
Sensitivity in the series configuration	$S_V^S = -1.632 \times 10^{-11} l$	
Acceleration Coefficient in the parallel configuration	$Q_P / \ddot{z} = -2.232 \times 10^{-5} l$	
Sensitivity in the parallel configuration	$S_V^P = -3.709 \times 10^{-11} l$	
Noise	$a_e = 4.4554 \times 10^{-8} (g) / \sqrt{Hz}$	
Minimum Detectable Signal (MDS) (Resolutions)	$MDS = 5.0556 \times 10^{-8} (g)$	
Maximum Detectable Range	$\ddot{z}_{max} = 3.0413 \times 10^4 (g)$	

Chapter 4
Simulation of Bridge-Type Capacitive Micro Accelerometer

4.1   Introduction

Bridge-type capacitive micro accelerometer is a type of popular transducer used to measure acceleration in a great variety conditions. Up to now, the bridge-type capacitive micro accelerometer has achieved a lot of development. Through analysis and comparison between it and the bridge-type micro accelerometer with two piezoelectric thin films read-out, the performances of these two types of accelerometers will be found and they can be used into the different application field according to their different performances.

In Chapter 3, the analysis of bridge-type capacitive micro accelerometer has been done and the formulas of the properties have been obtained. In this chapter, the analytical model of bridge-type capacitive micro accelerometer will be analyzed. After that, CoventorWare 2004 will be used to do the FEM analysis of the imaginary model to prove our calculation.

4.2   Analytical Solution of Bridge-type Capacitive Micro Accelerometer

4.2.1   Assumption

The following assumptions are made in the model of this section:

1) Compared with the central seismic mass, the mass of the beams are too small they can be ignored;

2) The central seismic mass and rim of the whole structure are rigid;

3) The beams are elastic and they obey Hooke's law;

4) The whole structure is symmetrical.

The directions are defined as Figure 4.1.
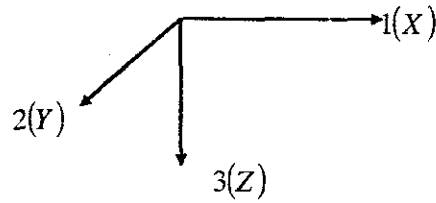
Figure 4.1: Direction of the coordination

4.2.2   Formulas of Bridge-type Capacitive Micro Accelerometer

The structure of bridge-type capacitive micro accelerometer has the two beams fixed on each end, and each beam's performance is shown in Figure 4.2.
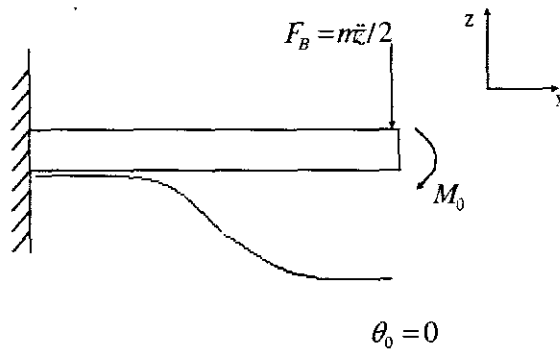
Figure 4.2: The deformation of the suspending beam

When the acceleration is induced on the seismic central mass, the reaction force induces a deflection on the suspending beam. Because of this, it follows that the force equilibrium along three directions should be given by the following reaction force:

$$F_B = \frac{1}{2}m\ddot{z} \tag{4.1}$$

Where m is central mass.

From the boundary conditions, we have the real bending moment:

$$M = M_0 - \frac{1}{2}Fx \qquad (4.2)$$

Where M_0 is assumptive bending moment.

From Figure 4.2, we can see that when the displacement up to max, the rotation angle of the end (θ_l) which is connected with concentrative mass is still 0 ($\theta_l = 0$) since the mass will never bend. (δ is the max displacement)

In terms of the particularity of this structure (two sides fixed) we use the theorem of energy--*Castigliano's Theorem* to require the max displacement of the beam in succession.

The denotation of strain energy is U.

$$U = \int_0^l \frac{M^2}{2EI_z} dx \qquad (4.3)$$

Where $I_z = \frac{bh^3}{12}$ and I_z is the moment of inertia to the axis z.

Apply $\theta_0 = 0$ to require bending moment

$$\theta_0 = \frac{\partial U}{\partial M_0} = \int_0^l \frac{M}{EI_z} \frac{\partial M}{\partial M_0} dx = \frac{1}{EI_z} \int_0^l \left(M_0 - \frac{1}{2}Fx \right) dx = 0 \qquad (4.4)$$

By solving this equation, the bending moment is shown as:

$$M_0 = \frac{1}{4}Fl \qquad (4.5)$$

and

$$M = \frac{1}{4}Fl - \frac{1}{2}Fx = \frac{1}{2}F(\frac{l}{2} - x) \qquad (4.6)$$

Then the max displacement will be:

$$\delta = \frac{\partial U}{\partial F_B} \int_0^l \frac{M}{EI_z} \frac{\partial M}{\partial F_B} dx = \frac{F}{2EI_z} \int_0^l \left(\frac{l}{2} - x \right)^2 dx = \frac{Fl^3}{24EI_z} \qquad (4.7)$$

And substitute $I_z = \frac{bh^3}{12}$ into Eq.(4.7), we finally have:

$$\delta = \frac{Fl^3}{2Ebh^3} = \Delta\delta \qquad (4.8)$$

Substitute $F = m\ddot{z}$ into Eq.(4.8):

$$\Delta\delta = \frac{m\ddot{z}l^3}{2Ebh^3} \qquad (4.9)$$

Initial capacitance is C_0:

$$C_0 = \frac{\varepsilon_0 s}{\delta_0} \qquad (4.10)$$

Where ε_0 is dielectric constant, s is relative area between two electrode plate and δ_0 is initial distance between two electrode plate.

During the course of design, the relative area between two plates can be kept unchangeable, if the area of bottom plate (s_b) is less than the area of top plate (s_r). So the change of distance between two plates will be concerned only.

The capacitance after δ_0 has changed to C_1:

$$C_1 = \frac{\varepsilon_0 s}{\delta_0 - \Delta\delta} \qquad (4.11)$$

Substitute Eq.(4.9) into this formula, we have:

$$C_1 = \frac{2\varepsilon_0 sEbh^3}{2Ebh^3\delta_0 - m\ddot{z}l^3} \tag{4.12}$$

So we can obtain the change of capacitance:

$$\begin{aligned}
\Delta C &= C_1 - C_0 \\
&= \frac{2\varepsilon_0 sEbh^3}{2Ebh^3\delta_0 - m\ddot{z}l^3} - \frac{\varepsilon_0 s}{\delta_0} \\
&= \frac{2\varepsilon_0 sEbh^3\delta_0 - 2Ebh^3\delta_0\varepsilon_0 s + m\ddot{z}l^3\varepsilon_0 s}{2Ebh^3\delta_0^2 - m\ddot{z}l^3\delta_0} \\
&= \frac{m\ddot{z}l^3\varepsilon_0 s}{2Ebh^3\delta_0^2 - m\ddot{z}l^3\delta_0}
\end{aligned} \tag{4.13}$$

The result is hoped too be a linear expression, so the next work is to simplify this complex result to attain a linear expression.

$$\begin{aligned}
\Delta C &= C_1 - C_0 = \frac{\varepsilon_0 s}{\delta_0 - \Delta\delta} - \frac{\varepsilon_0 s}{\delta_0} \\
&= \varepsilon_0 s\Delta\delta\left(\frac{1}{\delta_0 - \Delta\delta}\right) \\
&= \varepsilon_0 s\Delta\delta\left(\frac{\frac{1}{\delta_0}}{1 - \frac{\Delta\delta}{\delta_0}}\right) \\
&= \varepsilon_0 s\frac{\Delta\delta}{\delta_0}\left(\frac{1}{1 - \frac{\Delta\delta}{\delta_0}}\right)
\end{aligned} \tag{4.14}$$

When the expression $\dfrac{\Delta\delta}{\delta_0} \ll 1$ comes into existence, we can do a transform through the series to simplify it.

At first, we spread $\left(1 - \dfrac{\Delta\delta}{\delta_0}\right)^{-1}$ into a Fourier series:

$$\left(1-\frac{\Delta\delta}{\delta_0}\right)^{-1}=1+\frac{\Delta\delta}{\delta_0}+\left(\frac{\Delta\delta}{\delta_0}\right)^{2}+\left(\frac{\Delta\delta}{\delta_0}\right)^{3}+\ldots+\left(\frac{\Delta\delta}{\delta_0}\right)^{n}$$

This formula is nonlinear, so nonlinear terms can be omitted and the approximate formula will be:

$$\Delta C = \varepsilon_0 s \frac{\Delta\delta}{\delta^2} \tag{4.15}$$

Finally, the relationship between $\ddot{z}$ and ΔC can be obtained:

$$\Delta C = \frac{ml^3 \varepsilon_0 s}{2Ebh^3 \delta_0^2}\ddot{z} \tag{4.16}$$

and

$$\ddot{z} = \frac{2Ebh^3 \delta_0^2}{ml^3 \varepsilon_0 s}\Delta C \tag{4.17}$$

From Eqs.(4.16) and (4.17), we can see that there is a linear relationship between the acceleration $\ddot{z}$ and the capacitive change ΔC, and the equations include dielectric constant ε_0, elastic coefficient E, thickness h for the beam, length l and width b for the beam, relative area between two electrode plate s, and initial distance between two electrode plates δ_0. So we can adjust any of these parameters to increase or decrease the output.

4.2.3 Sensitive Analysis

Sensitivity is a very important and practical parameter of sensors. It is the feature cared firstly when customers choose a type of sensor. So the accurate range of sensitivity of sensors must be found and comfirmed.

The sensitivity of bridge-type capacitive micro accelerometers is defined as the ratio of the capacitance change ΔC and the displacement change of the electrode plate $\Delta\delta$: Then the sensitivity of the bridge-type capacitive micro accelerometer will be:

$$S_{V1} = \frac{\Delta C}{\Delta \delta} = \frac{\varepsilon_0 s}{\delta_0^2} \qquad (4.18)$$

Similar to the acceleration equation, the sensitivity equation includes the acceleration $\ddot{z}$ and the capacitance change ΔC, and the equations include dielectric constant ε_0, relative area between two electrode plates s, and initial distance between two electrode plates δ_0. So we can adjust any of these parameters to increase or decrease the output.

Another definition of the sensitivity is the rate between the input and the output of the device. So the sensitivity of the bridge-type capacitive micro accelerometer can also be calculated as:

$$S_{V2} = \frac{\Delta C}{\ddot{z}} = \frac{ml^3 \varepsilon_0 s}{2Ebh^3 \delta_0^2} \qquad (4.19)$$

Sometimes to improve the sensitivity of sensors, difference configuration can be adopted. Figure 4.3 is a more complicated structure than that proposed in this thesis.
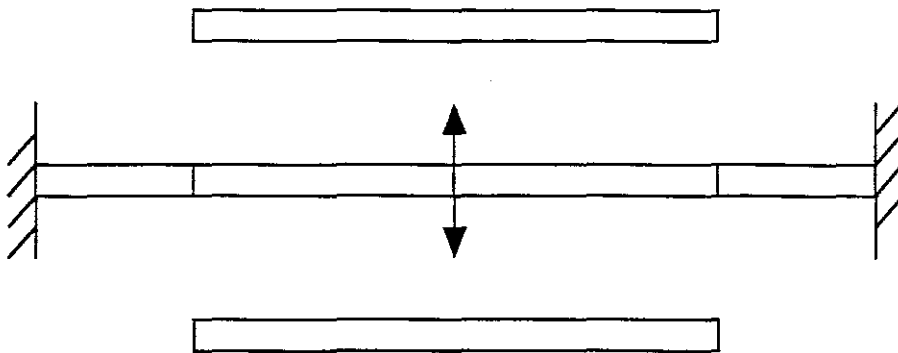

Figure 4.3: the sketch map of difference configuration

When the central electrode plate moves up and down, the capacitance between upper and lower electrode plates will change at the same time. Then the change of

capacitance between upper and center electrode plates will equal to that between center and lower electrode plates. It means the change of capacitance that we detect will be two times of the one of the structure that we introduced before.

$$\Delta C' = 2\Delta C$$

At this time, the sensitivity will equal to two times S which we have acquired already.

$$S_{V1}' = 2S_{V1} = 2\frac{\Delta C}{\Delta \delta} = 2\frac{\varepsilon_0 s}{\delta_0^2} \tag{4.20a}$$

$$S_{V2}' = 2S_{V2} = \frac{2\Delta C}{\ddot{z}} = \frac{ml^3 \varepsilon_0 s}{Ebh^3 \delta_0^2} \tag{4.20b}$$

4.2.4 Natural Frequency Analysis

The accelerometer is an inertia system. So the device can be transformed to a equivalent mass-spring inertia system. The device follows the elastic formula:

$$F = kx \tag{4.21}$$

In Eq.(4.21), we consider $x = \Delta \delta$, then Eq.(4.9) can transform to:

$$x = \frac{Fl^3}{2Ebh^3}$$

Then

$$k = \frac{F}{x} = \frac{2Ebh^3}{l^3} \tag{4.22}$$

To inertia system, the natural frequency can calculate as:

$$f = \frac{1}{2\pi}\sqrt{\frac{k}{m}} \tag{4.23}$$

Substituting Eq.(4.22) into Eq.(4.23), the formula will become to:

$$f = \frac{1}{2\pi} \sqrt{\frac{2Ebh^3}{ml^3}} \tag{4.24}$$

4.2.4 Noise Analysis

Same as the bridge-type micro accelerometer with two piezoelectric thin films read-out, the Brownian noise is a mainly impact for the measurement and must be considered when it is designed.

The Brownian noise equivalent acceleration of the system is

$$a_e = \frac{\sqrt{4k_BTD}}{m} \tag{4.25}$$

Where k_B is Boltzmann's constant ($k_B = 1.38 \times 10^{-23} J / K$), D is damping coefficient and T is absolute temperature ($T = 300K$).

The exact value of the damping coefficient D does not need to be computed and can be dominated with the quality factor, Q, of the system under harmonic excitation according the following formula:

$$D = \frac{\sqrt{km}}{Q} \tag{4.26}$$

Where k is the elastic coefficient of the system and m is the general mass.

And the value of the quality factor follows the formula:

$$Q = \frac{d\sqrt{mk}}{\mu_0 A} \tag{4.27}$$

Where d is the gap between the mass and the substrate, A is the area of horizontal cross-section of the mass and μ_0 is the viscosity of air at 27°C ($\mu_0 = 18 \times 10^{-6} kg / m \cdot s$)

Substituting Eqs.(4.22) and (4.23) into Eq(4.21), the Brownian noise equivalent acceleration of the system is shown as:

$$a_e = \sqrt{\frac{4\mu_0 k_B TA}{dm^2}} \tag{4.28}$$

4.2.5 Minimum Detectable Signal

The minimum detectable signal (MDS) is a very useful parameter for the sensors. Knowledge of the MDS is also necessary when calculating the dynamic range or signal to noise ratio for a particular receiver configuration. The following treatment outlines a straightforward method to derive the MDS:

$$MDS = \frac{N_0 \times \sqrt{BW}}{S_V} \tag{4.29}$$

The thermal noise equivalent voltage spectral density is defined as follow:

$$N_0 = a_e S_V \tag{4.30}$$

The bandwidth of the system is:

$$BW = \frac{\sqrt{k/m}}{Q} \tag{4.31}$$

Then substituting Eqs.(4.23), (4.26) and (4.27) into Eq.(4.25), the minimum detectable signal will be obtained:

$$
\begin{aligned}
MDS &= \frac{N_0 \times \sqrt{BW}}{S_V} \\
&= \frac{\sqrt{4k_B TDBW}}{m} \\
&= \frac{\mu_0 A}{d} \times \sqrt{\frac{4k_B T}{m^3}}
\end{aligned} \tag{4.32}
$$

4.2.7 Dynamic Analysis

The dynamic model is subjected to a periodic force $f(t)$, as shown schematically by Figure 4.4. The sinusoidal force can be written as:

$$f(t) = mg \sin 2\pi f t \tag{4.33}$$

Where $g = 9.8 m/s$ and f is the driving frequency.
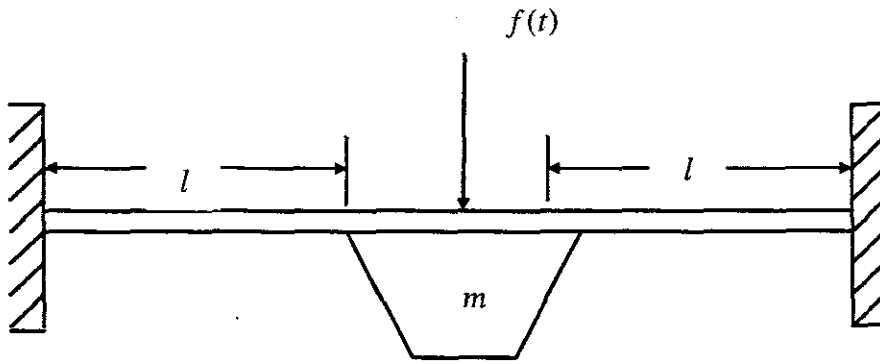
Figure 4.4: Dynamic model of accelerometer

Causing only the first vibration mode is considered, the general solution of the beam is given by [McCallion, 1973]

$$z(x) = a_1 \cos(\beta x) + a_2 \sin(\beta x) + a_3 \cosh(\beta x) + a_4 \sinh(\beta x) \tag{4.34}$$

Where a_1, a_2, a_3, a_4, β are constants.

From the boundary conditions, the first normal mode of the accelerometer can be obtained as:

$$z_1(x) = V_a[\sin kx - \sinh(kx) + S(\cos kx - \cosh(kx))]$$
$$= V_a g(x)$$

Where $k = 4.73/2l$

$$S = \frac{(\sinh(kl) - \sin kl)}{(\cos kl - \cosh(kl))} \tag{4.35}$$

and V_a is the constant.

Since the first normal is orthogonal, V_a can be obtained by

$$\int_0^{2l} \gamma(x)A(x)z_1^2(x)dx = 1 \tag{4.36}$$

Where $\gamma(x)$ is the density and A is the cross-sectional area.

Assuming that the seismic mass m is much larger that the mass of the beam, the above equation can then be simplified

$$V_a = \sqrt{\frac{g^2(l)}{m}} \tag{4.37}$$

From Rayleigh method, the fundamental natural frequency f_n is given by

$$f_n^2 = 2\int_0^l \frac{dU_{max}}{4\pi^2 K_{e\,max}} \tag{4.38}$$

In which $K_{e\,max} = mz_1^2(l)$

For beam with single elastic layer, we have

$$dU_{max} = \frac{1}{2}\left(\frac{d^2z_1}{dx^2}\right)^2 EI \tag{4.39}$$

Using the expansion theorem, the displacement of the accelerometer is

$$z(x,t) = z_1(x)\eta(t) \tag{4.40}$$

$\eta(t)$ is the modal coordinate given by

$$\eta(t) = \frac{1}{2\pi f_n}\left(\int_0^t N(\tau)\sin(2\pi f_n)(t-\tau)d\tau\right) \tag{4.41}$$

And N is the modal force given by

$$N(t) = \int_0^{2l} z_1(x) f(x,t) dx \tag{4.42}$$

Substituting Eqs.(4.29), (4.37) and (4.38) into Eq.(4.36), we have

$$z(x,t) = \frac{V_a^2 mgz(l)\left[\sin 2\pi f t - (f/f_n)\sin 2\pi f_n t\right]}{(2\pi f_n)^2 - (2\pi f)^2} \\ \times \left[\sin kx - \sinh(kx) + S(\cos kx - \cosh(kx))\right] \tag{4.43}$$

Substituting the Eq.(4.43) into Eq.(4.16), the dynamic equation of capacitance change can be acquired:

$$\Delta C = \frac{ml^3 \varepsilon_0 s}{2Ebh^3 \delta_0^2} \times \frac{V_a^2 mg\ddot{z}(l)\left[\sin 2\pi f t - (f/f_n)\sin 2\pi f_n t\right]}{(2\pi f_n)^2 - (2\pi f)^2} \\ \times \left[\sin kl - \sinh(kl) + S(\cos kl - \cosh(kl))\right] \tag{4.44}$$

Using this equation, the capacitance change (ΔC) and acceleration ($\ddot{z}$) of the device under dynamic excitation can be predicted.

4.2.8   Stress Analysis

As Eq.(4.2) shown, the maximum of moment is at $x = 0$. Assuming there is only vertical acceleration applied to the central seismic mass, the beams are primarily subjected to stresses in the one-direction, and the other stresses are too small and can be ignored. Therefore, the maximum stress can be obtained:

$$\sigma_{max} = \frac{E}{1 - \mu^2} \frac{m\ddot{z}_{max} l^2}{16EI_z} \tag{4.45}$$

Then the maximum detectable range can be calculated by:

$$\ddot{z}_{max} = \frac{4bh^3 (1 - \mu^2) \sigma_{max}}{3ml^2} \tag{4.46}$$

4.2.9 Numerical Calculation

To gain an intuitionist result, the parameters of the accelerometers can be calculated according the above formulations. The geometry of the accelerometer structure used for the proposed modeling is given in Table 4.1. And the mechanical properties of the accelerometer materials are shown as Table 4.2.

In this thesis, since the area of upper electrode plate is bigger than bottom one, the area of the bottom electrode plate is considered only when the relative area between these two plates is calculated.

Table 4.1: Dimension of capacitive accelerometer

Length of suspension beam, l (μm)	700
Width of suspension beam, b (μm)	200
Thickness of suspension beam, h (μm)	5
Gap between the mass and substrate, δ_0 (μm)	20
Length of seismic mass, l_m (μm)	400
Width of seismic mass, b_m (μm)	400
Thickness of seismic mass, h_m (μm)	300
Length of the electrode, l_e (μm)	350
Width of the electrode, b_e (μm)	350

Table 4.2: Mechanical properties of the materials

	Silicon
Young's modulus (N/m^2)	1.9×10^{11}
Poisson's ratio	0.18
Density (kg/m^3)	2330
Fracture strength (N/m^2)	7×10^9 [Peterson, 1982]

The seismic mass will be:

$$m = V_m \rho$$
$$= l_m b_m h_m \rho$$
$$= 400 \times 10^{-6} \times 400 \times 10^{-6} \times 300 \times 10^{-6} \times 2330$$
$$= 1.1184 \times 10^{-7} kg$$

From Eq.(4.22), the equivalent elastic coefficient should be:

$$k = \frac{2Ebh^3}{l^3}$$

$$= \frac{2 \times 1.9 \times 10^{11} \times 200 \times 10^{-6} \times \left(5 \times 10^{-6}\right)^3}{\left(700 \times 10^{-6}\right)^3}$$

$$= 27.6968 N/m$$

Then the quality factor and bandwidth can be obtained:

$$Q = \frac{d\sqrt{mk}}{\mu_0 A}$$

$$= \frac{d\sqrt{km}}{\mu_0 l_m b_m}$$

$$= \frac{20 \times 10^{-6} \times \sqrt{1.1184 \times 10^{-7} \times 27.6968}}{18 \times 10^{-6} \times 400 \times 10^{-6} \times 400 \times 10^{-6}}$$

$$= 1.2222 \times 10^4$$

$$BW = \frac{\sqrt{k/m}}{Q}$$

$$= \frac{\sqrt{\dfrac{27.6968}{1.1184 \times 10^{-7}}}}{1.2222 \times 10^4}$$

$$= 1.2876 Hz$$

And the natural frequency of the system is:

$$f = \frac{1}{2\pi}\sqrt{\frac{k}{m}}$$

$$= \frac{1}{2\pi}\sqrt{\frac{27.6968}{1.1184 \times 10^{-7}}} \qquad (4.47)$$

$$= 2.5046 kHz$$

Although the structure of bridge-type capacitive accelerometer is similar with bridge-type accelerometer with two piezoelectric thin films read-out, it has no influence of piezoelectric thin films. So the frequency of bridge-type capacitive micro

accelerometer is smaller than that of bridge-type micro accelerometer with two piezoelectric thin films read-out.

The acceleration equation can be calculated through Eq.(4.16):

$$\Delta C = \frac{ml^3 \varepsilon_0 s}{2Ebh^3 \delta_0^2} \ddot{z}$$

$$= \frac{ml^3 \varepsilon_0 l_e b_e}{2Ebh^3 \delta_0^2} \ddot{z} \qquad\qquad (4.48)$$

$$= \frac{1.1184\times10^{-7} \times (700\times10^{-6})^3 \times 8.85\times10^{-12} \times 350\times10^{-6} \times 350\times10^{-6}}{2\times1.9\times10^{11} \times (5\times10^{-6})^3 \times (20\times10^{-6})^2} \ddot{z}$$

$$= 1.0944\times10^{-17} \ddot{z}$$

So

$$\ddot{z} = \frac{2Ebh^3 \delta_0^2}{ml^3 \varepsilon_0 s} \Delta C$$

$$= \frac{2Ebh^3 \delta_0^2}{ml^3 \varepsilon_0 l_e b_e} \Delta C \qquad\qquad (4.49)$$

$$= \frac{2\times1.9\times10^{11} \times (5\times10^{-6})^3 \times (20\times10^{-6})^2}{1.1184\times10^{-7} \times (700\times10^{-6})^3 \times 8.85\times10^{-12} \times 350\times10^{-6} \times 350\times10^{-6}} \Delta C$$

$$= 9.3235\times10^{15} \Delta C (g)$$

And from Eqs.(4.18) and (4.19), the sensitivity of two configurations is shown as:

$$S_{V1} = \frac{\varepsilon_0 s}{\delta_0^2}$$

$$= \frac{\varepsilon_0 l_e b_e}{\delta_0^2}$$

$$= \frac{8.85\times10^{-12} \times 350\times10^{-6} \times 350\times10^{-6}}{(20\times10^{-6})^2}$$

$$= 2.7103\times10^{-9} \, F/m$$

$$S_{V2} = \frac{ml^3 \varepsilon_0 s}{2Ebh^3 \delta_0^2}$$

$$= \frac{ml^3 \varepsilon_0 l_e b_e}{2Ebh^3 \delta_0^2}$$

$$= \frac{1.1184 \times 10^{-7} \times (700 \times 10^{-6})^3 \times 8.85 \times 10^{-12} \times 350 \times 10^{-6} \times 350 \times 10^{-6}}{2 \times 1.9 \times 10^{11} \times (5 \times 10^{-6})^3 \times (20 \times 10^{-6})^2}$$

$$= 1.0944 \times 10^{-17} \, F \cdot s^2 / m$$

$$= 1.0725 \times 10^{-16} \, F / (g)$$

From Eqs.(4.28) and (4.32), the Brownian noise equivalent acceleration and MDS can be obtained:

$$a_e = \frac{\sqrt{4k_B TD}}{m}$$

$$= \frac{\sqrt{4k_B T \frac{\sqrt{km}}{Q}}}{m}$$

$$= \frac{\sqrt{4 \times 1.38 \times 10^{-23} \times 300 \times \frac{\sqrt{27.6968 \times 1.1184 \times 10^{-7}}}{1.2222 \times 10^4}}}{1.1184 \times 10^{-7}}$$

$$= 4.4554 \times 10^{-8} (g) / \sqrt{Hz}$$

$$MDS = \frac{\mu_0 A}{d} \times \sqrt{\frac{4k_B T}{m^3}}$$

$$= \frac{\mu_0 l_m b_m}{d} \times \sqrt{\frac{4k_B T}{m^3}}$$

$$= \frac{18 \times 10^{-6} \times 400 \times 10^{-6} \times 400 \times 10^{-6}}{20 \times 10^{-6}} \times \sqrt{\frac{4 \times 1.38 \times 10^{-23} \times 300}{(1.1184 \times 10^{-7})^3}}$$

$$= 5.0556 \times 10^{-8} (g)$$

From Eq.(4.46), the maximum detectable range can be calculated:

$$\ddot{z}_{max} = \frac{4bh^3\left(1-\mu^2\right)\sigma_{max}}{3ml^2}$$

$$= \frac{4\times200\times10^{-6}\times\left(5\times10^{-6}\right)^3\times\left(1-0.18\right)^2\times7\times10^9}{3\times1.1184\times10^{-7}\times\left(700\times10^{-6}\right)^2}$$

$$= 4.11845\times10^3\, m/s^2$$

$$= 4.2025\times10^2\left(g\right)$$

(4.50)

Comparing the two types of bridge-type micro accelerometers, the bridge-type capacitive micro accelerometer is more sensitive and the bridge-type micro accelerometer with two piezoelectric thin films read-out can be used to detect larger acceleration.

Substituting Eq.(4.50) into Eq.(4.9), we can get the maximum displacement under the maximum stress loaded:

$$\Delta\delta_{max} = \frac{m\ddot{z}_{max}l^3}{2Ebh^3}$$

$$= \frac{1.1184\times10^{-7}\times4.11945\times10^3\times\left(700\times10^{-6}\right)^3}{2\times1.9\times10^{11}\times200\times10^{-6}\times\left(5\times10^{-6}\right)^3}$$

$$= 2.3763\times10^{-8}\,m$$

$$= 23.763nm$$

(4.51)

Comparing the maximum displacement under the maximum stress loaded with the gap between the two electrode plates, it is much smaller than the gap. So the maximum detectable range should be:

$$\ddot{z}_{max} = 4.2025\times10^2\left(g\right)$$

(4.52)

4.3   Simulation with Software

In this Chapter, the simulation of accelerometers will be done. Because the program, Saber of CoventorWare 2004, can only simulate the capacitive sensor, simulating the bridge-type micro accelerometer with two piezoelectric thin films read-out has to be given up.

4.3.1 DC Operating Point Analysis

The operating point report can be obtained as Figure 4.5 shown:

In Figure 4.5, the elevation z is negative nonzero mainly due to the vertical asymmetry in the electric field lines at the electrodes, which produces a net (upwards) force in the negative z direction.

The DC Operating Point Analysis is a basic analysis for the following studies in the software: CoventorWare 2004.
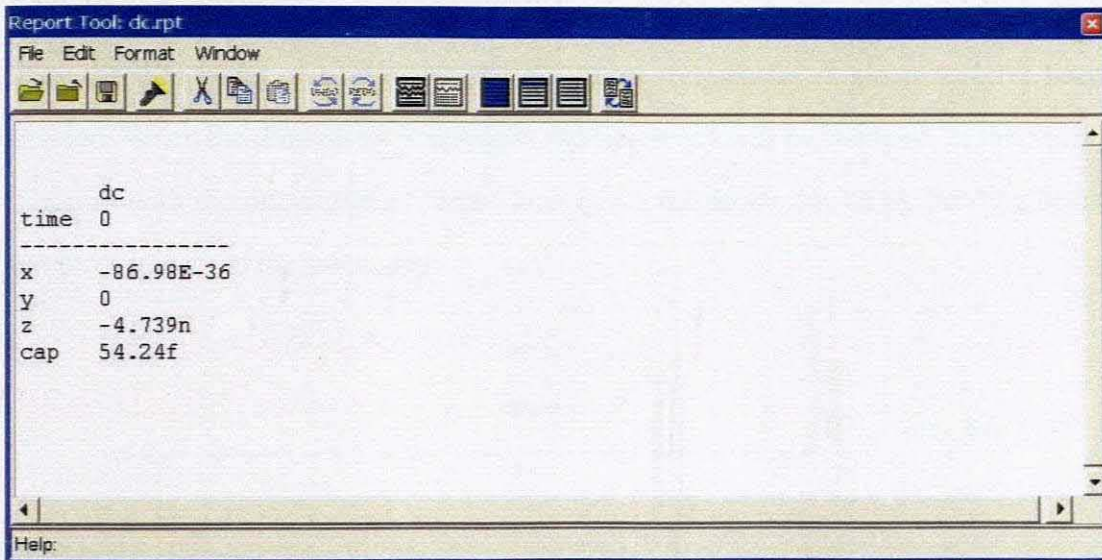

Figure 4.5: DC operating point analysis result

4.3.2 DC transfer (sweep) analysis

This analysis gives us the relationship of capacitance, displacement on z direction and voltage between two electrode plates (Figure 4.6). Here, the change of displacement and capacitance is caused from the static electric force produced by the voltage between two electrodes.
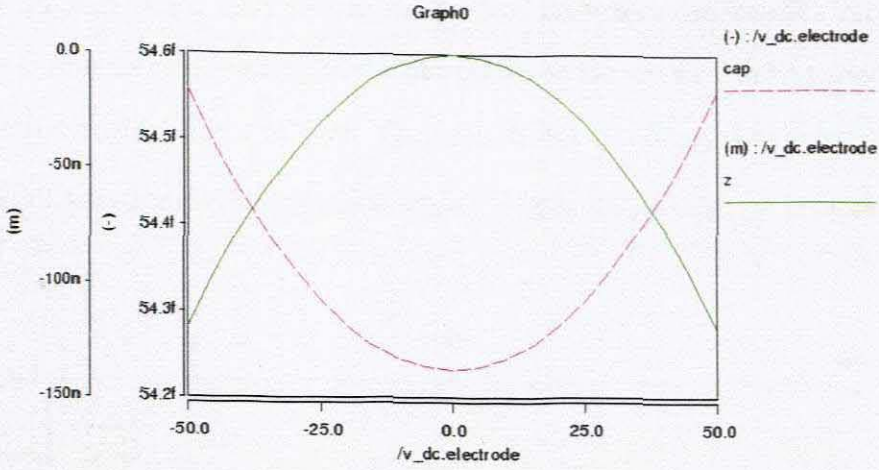
Figure 4.6: Relationship of capacitance, displacement and voltage

4.3.3 Resonance Frequencies

Once the dimension is determined, the resonance frequencies of structure have been decided. When the dimension is changed, the frequency will be changed. In this work, compare with the dimension of the seismic mass, the dimension of suspending beam has most impact of the frequency.
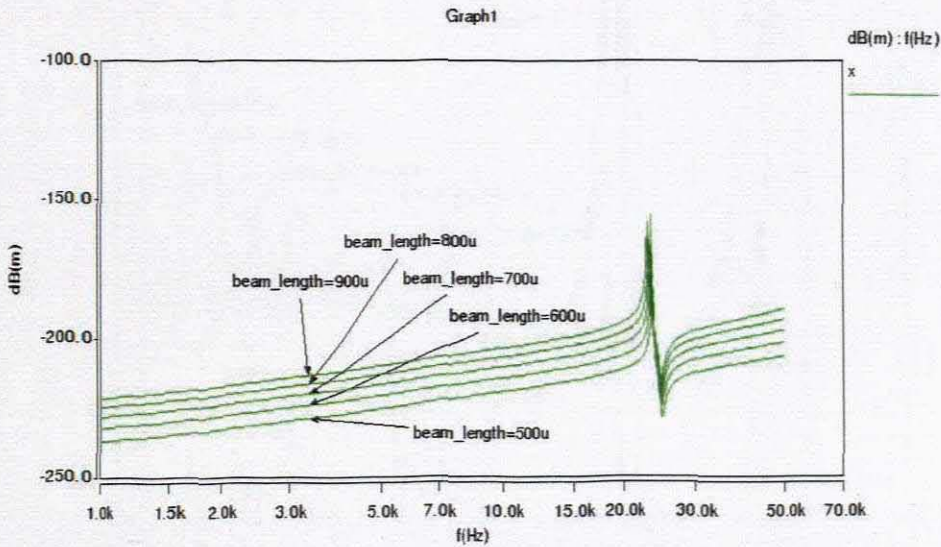

Figure 4.7: Resonance frequency (x axis) for varying beam length ($l = 500\mu m - 900\mu m$)

The following figures (Figure 4.7 to Figure 4.15) show the impact of the beam length, beam width and beam thickness to the system resonance frequencies on different directions. And using this analysis, the dimension of the device can be varied to make the vibration modes appear as wish. Then the device can be used to detect the signal on different direction, such as: translation on z axis, rotation on y axis etc.
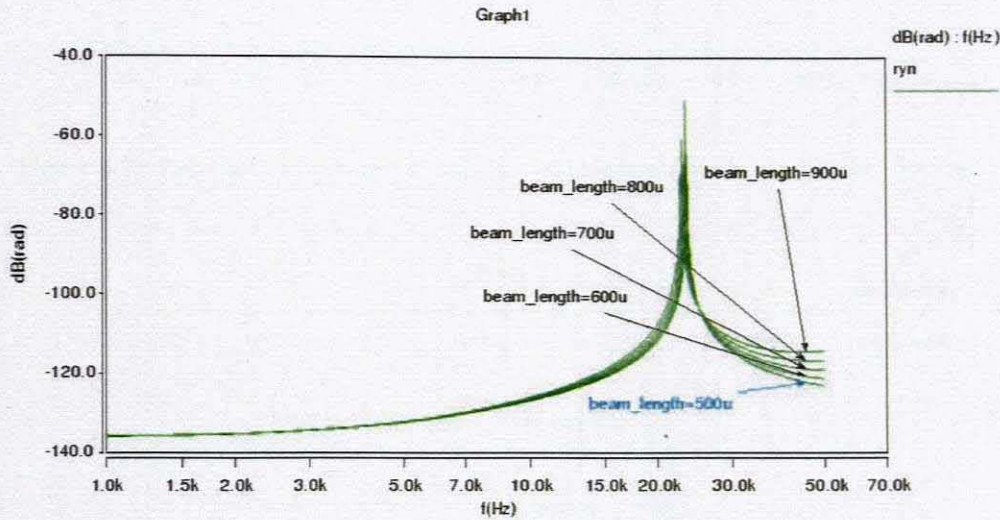

Figure 4.8: Resonance frequency (rotation on y axis) for varying beam length ($l = 500\mu m - 900\mu m$)
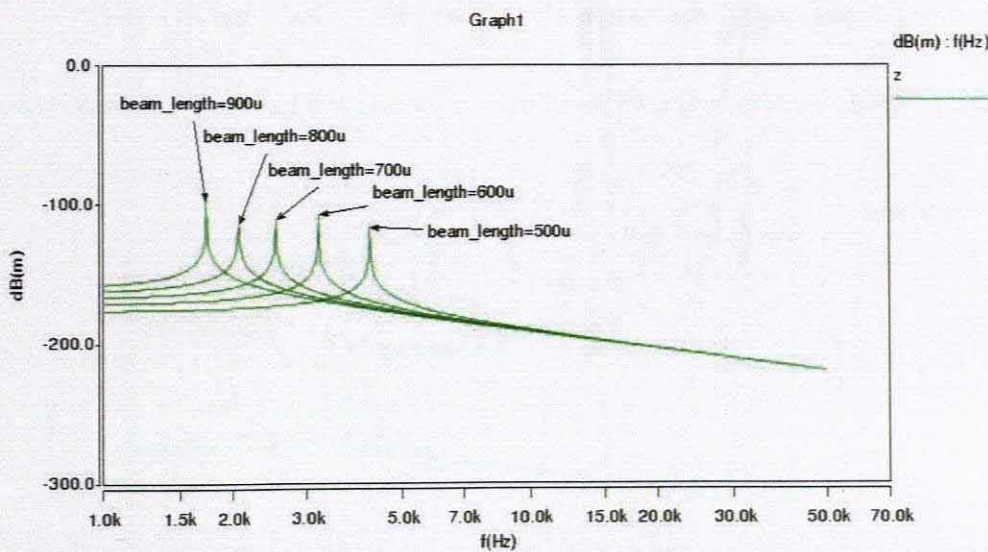
Figure 4.9: Resonance frequency (z axis) for varying beam length ($l = 500\mu m - 900\mu m$)
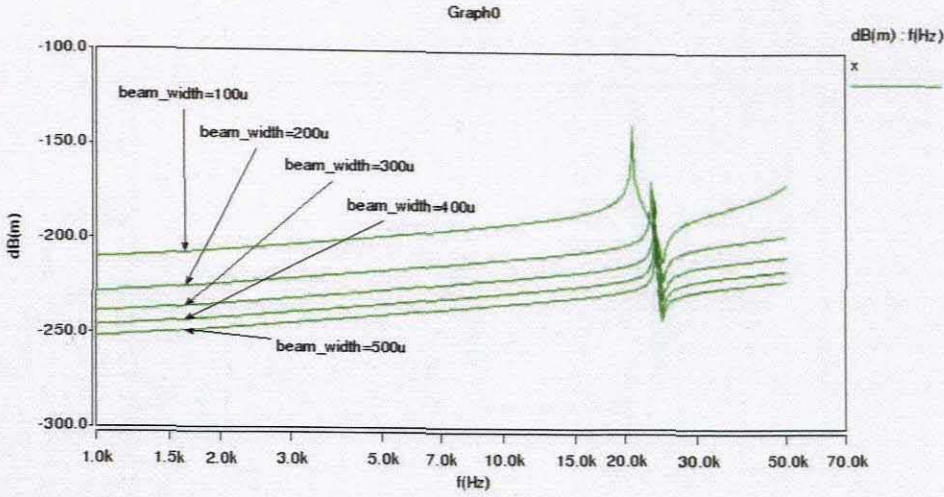
Figure 4.10: Resonance frequency (x axis) for varying beam width ($b = 100\mu m - 500\mu m$)
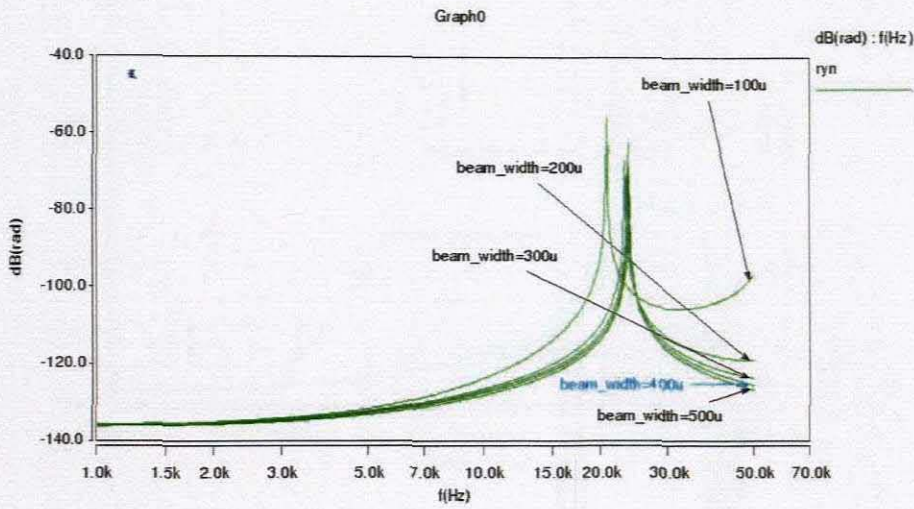
Figure 4.11: Resonance frequency (rotation on y axis) for varying beam width ($b = 100\mu m - 500\mu m$)
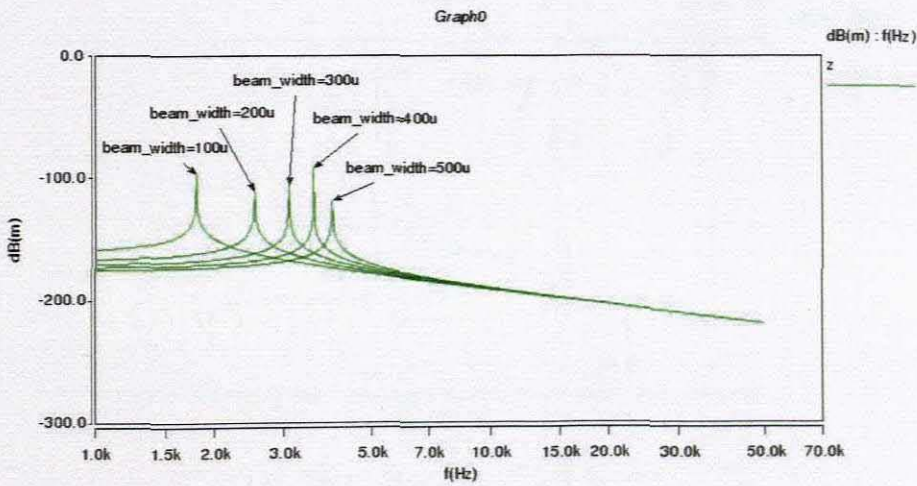
Figure 4.12: Resonance frequency (z axis) for varying beam width ($b = 100\mu m - 500\mu m$)
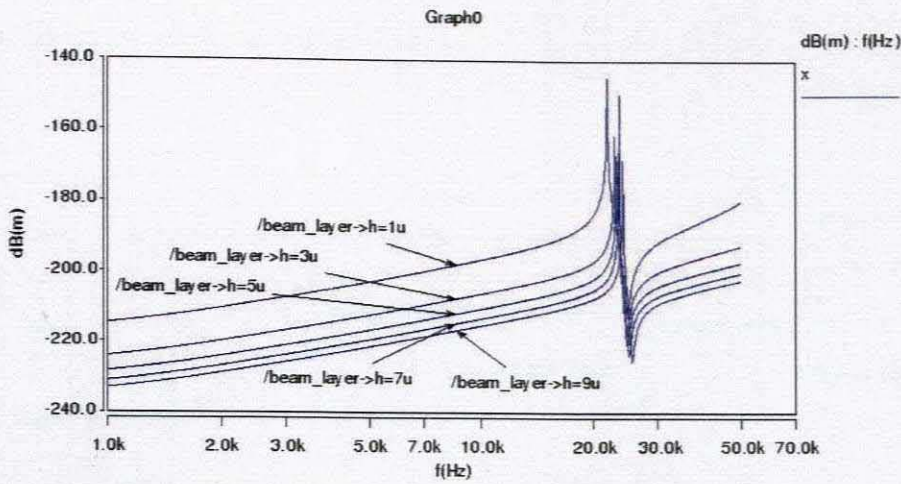
Figure 4.13: Resonance frequency (x axis) for varying beam thickness ($h = 1\mu m - 9\mu m$)
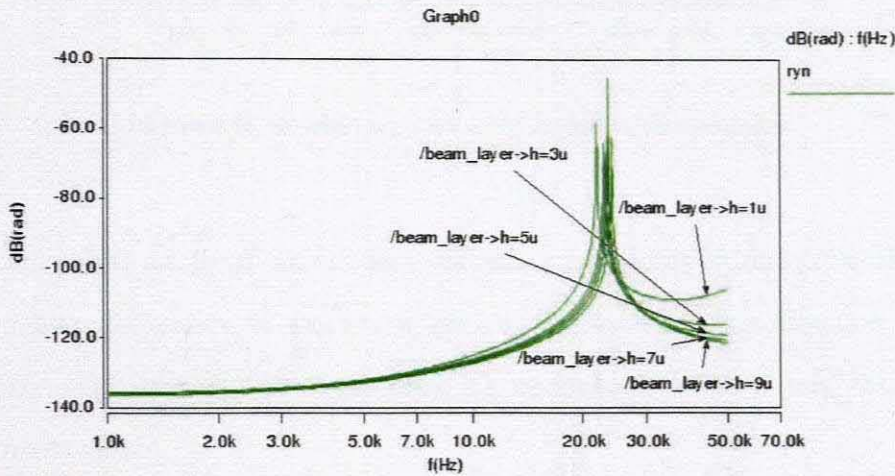
Figure 4.14: Resonance frequency (rotation on y axis) for varying beam thickness ($h = 1\mu m - 9\mu m$)
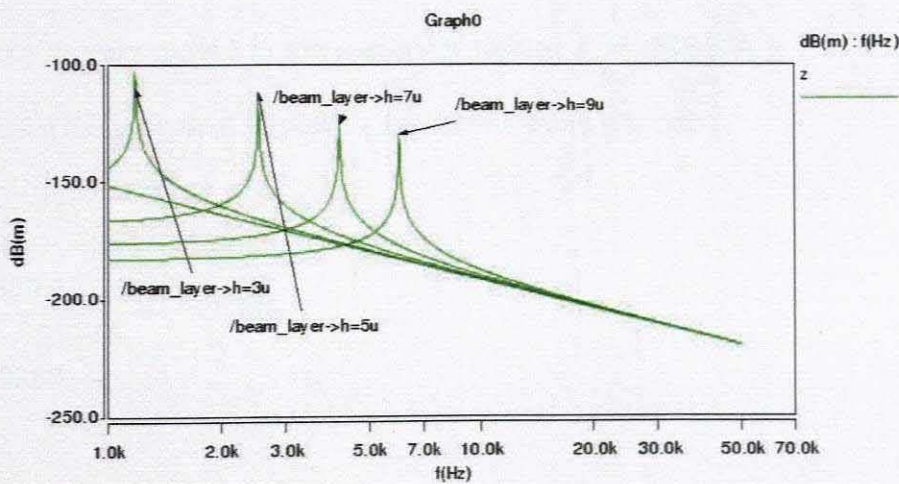
Figure 4.15: Resonance frequency (z axis) for varying beam thickness ($h = 1\mu m - 9\mu m$)

In this work the dimension is determined as Table 4.1. The resonance frequencies on

three directions are shown as Figure 4.16:
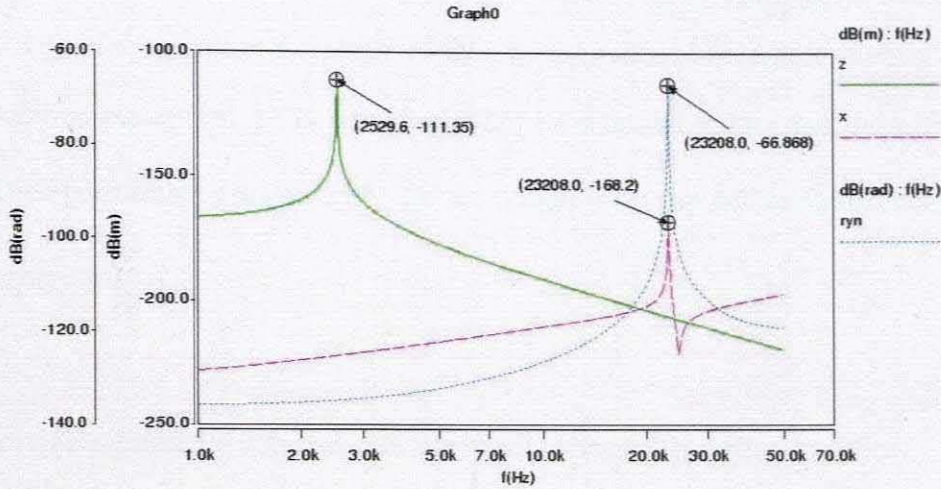
Figure 4.16: Resonance frequency of capacitive accelerometer

Which the points are lined out are the resonance frequencies on three directions. And

the resonance frequency of the whole device is that on z axis direction which is

2529.6Hz. Because the software uses an enumerate method, this result is an

approximate value.

Comparing with Eq.(4.47), the analytical result ($f_a = 2504.6Hz$) of the resonance

frequency is very closed to the numerical result ($f_c = 2529.6Hz$). The error (Δ) is

caused that the analytical formula is approximate and it is only:

$$\Delta = \frac{f_c - f_a}{f_c}$$
$$= \frac{2529.6 - 2504.6}{2529.6} \times 100\%$$
$$= 0.988\%$$

4.3.4 Sensitivity Analysis

The Sensitivity Analysis is an alternate and very effective method to study the impact of design parameters on a given performance parameter such as resonance frequency, dc point displacement, transient amplitude etc. With a sensitivity analysis the sensitivity of a parameter is calculated by a measurement-based perturbation method. A specified parameter p is perturbed from its nominal value, and the effect on a specified performance measure F for the design is determined as shown below:

$$sensitivity = \frac{\partial F}{\partial p}$$

To provide meaningful comparisons, the results are usually normalized:

$$sensitivity = \frac{\left(\frac{\Delta F}{F}\right)}{\left(\frac{\Delta p}{p}\right)} \Rightarrow \Delta F = sensitivity \cdot F \cdot \left(\frac{\Delta p}{p}\right)$$

Where p is the nominal value of the perturbed parameter, Δp is the amount by which the parameter is perturbed F is the nominal value of the performance measure and ΔF is the amount by which the performance measure changes in response to the parameter perturbation

In this report (shown in Figure 4.17), nominal value is the resonance frequency of the device. This is an exact resonance frequency. The resonance frequency of the driving mode is most sensitive to the design parameter beam_layer->h and beam_length.

A sensitivity of 1.5 means that a 1% perturbation of the beam thickness results in a $1.5 \times 1\% = 1.5\%$ decrease in the investigated resonance frequency. In absolute terms, increasing the beam thickness form $5 \mu m$ to $5.05 \mu m$ results in decrease of the resonance frequency of $1.5 \times No \min al \ Value \times 0.05 \mu m / 5 \mu m = 37.9 Hz$. And the

sensitivity of -1.48 means that a 1% perturbation of the beam length results in a $1.48 \times 1\% = 1.48\%$ increase in the investigated resonance frequency.
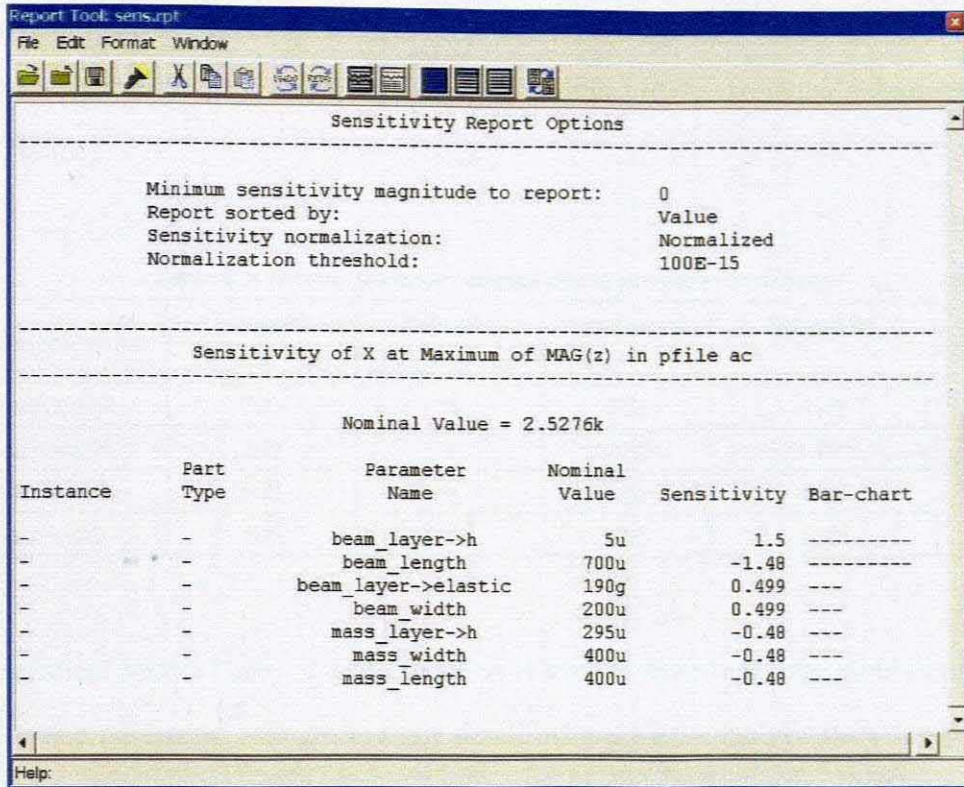
Figure 4.17: Sensitivity report

It is important to keep in perspective the absolute changes in parameters. A 1% change in the beam length is $7\mu m$, whereas a 1% change in beam thickness is $0.05\mu m$. Due to inaccuracies in fabrication process, the designer would most likely expect changes in the beam thickness lager than $0.05\mu m$ and changes in the beam length of much less than $7\mu m$. For this reason, it is worthwhile looking at the problem from a different perspective.

4.3.5 Monte Carlo Analysis

If the corresponding changes in key design parameters want to be known, expected changes in dimensions can be given, and then those dimensions with changes, which

push one or more of the key design parameters to fall outside the desirable performance regime, can be identified.

Fabrication-induced deviations of the in-plane dimensions are shown as Table 4.3, and the acceptable during frequency range is to within $10Hz$ from the nominal value ($2.5276kHz$).

Table 4.3: Driving frequency change due to parameter variations

Variable name	Nominal Value in μm	Expected change in μm	Perturbation	Sensitivity
Beam length	700	14	0.02	-1.48
Beam width	200	1	0.005	0.499
Mass length	400	4	0.01	-0.48
Mass width	400	4	0.01	-0.48

The statistical Monte Carlo analysis function is used to investigate the yield impact of the assumed parameter changes in more detail. Monte Carlo analysis uses component tolerances and statistical distributions to randomly vary system parameters during successive simulations.
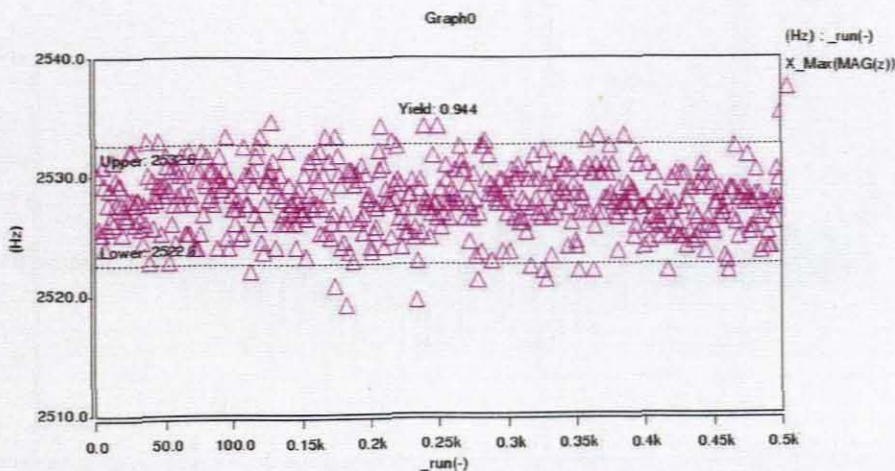
Figure 4.18: Monte Carlo Analysis

Figure 4.18 highlights the statistical probability of certain frequencies. The graph on the bottom shows the measured frequency points for each of the 500 sample points of Monte Carlo run. The results of the yield analysis indicate that 94.4% of the device samples will have a driving frequency within the required limit of the nominal value $\pm 5Hz$.

4.3.6   Transient Analysis

In this section, a transient analysis is performed in which the driving signal is a sinusoidal voltage with amplitude of $2V$, frequency equal to its natural frequency.

Figure 4.19 to Figure 4.25 show the capacitive, translation and rotation transient analysis results on three axis directions.

The amplitude of the driving motion (z) is slowly declining over time. This may be surprising because the in-plane mode was excited at its resonance frequency. The reason for this behavior is called numerical damping, which is an intrinsic property of numerical transient solvers.

Figure 4.19: Transient Analysis of translation on x axis

Figure 4.20: Transient Analysis of translation on y   axis
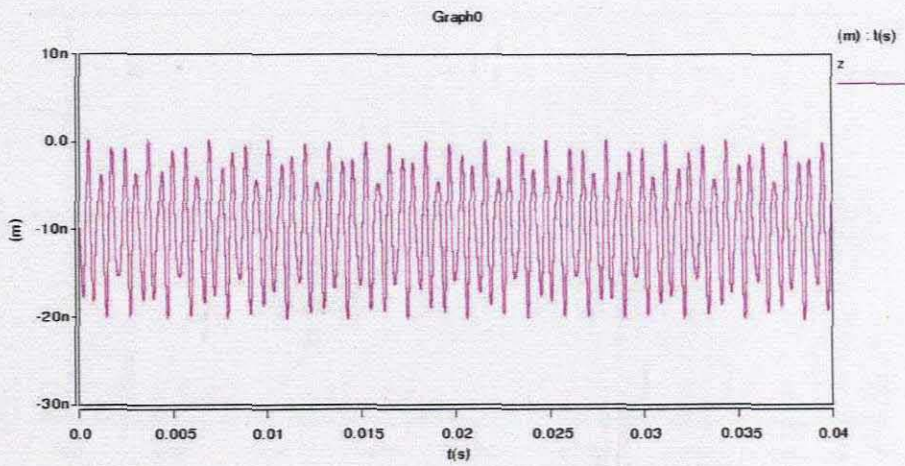
Figure 4.21: Transient Analysis of translation on z   axis
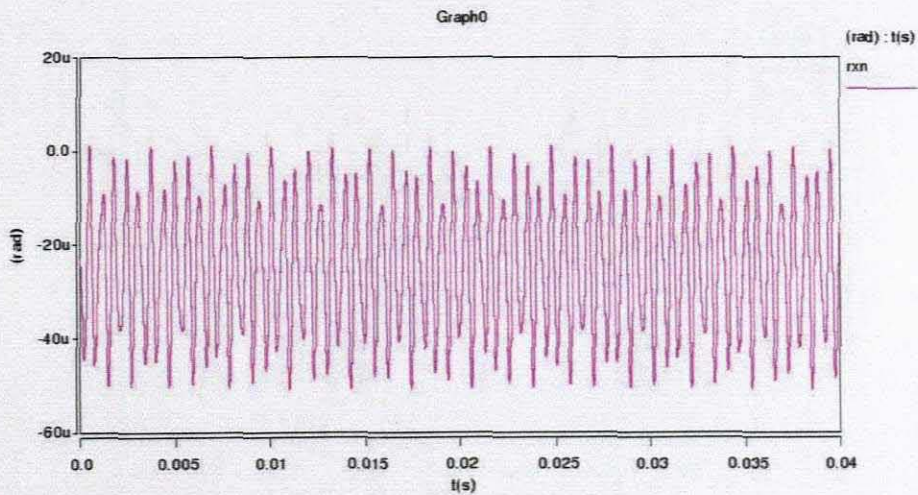
Figure 4.22: Transient Analysis of rotatation on x   axis
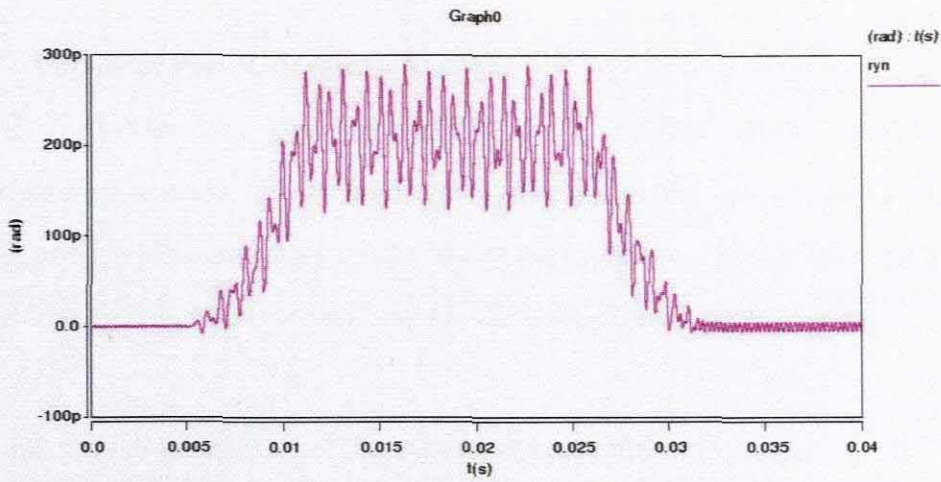
Figure 4.23: Transient Analysis of rotatation on y   axis
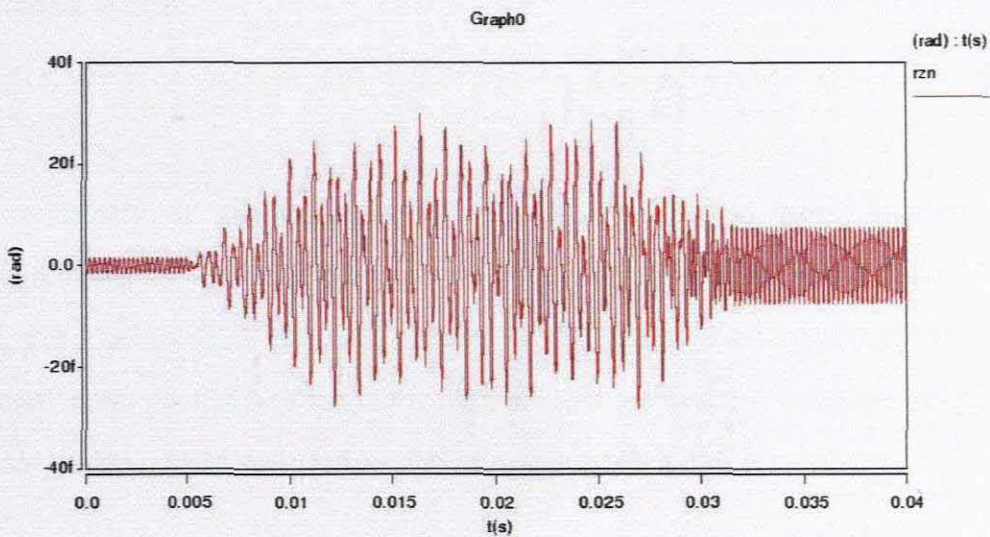
Figure 4.24: Transient Analysis of rotatation on z   axis
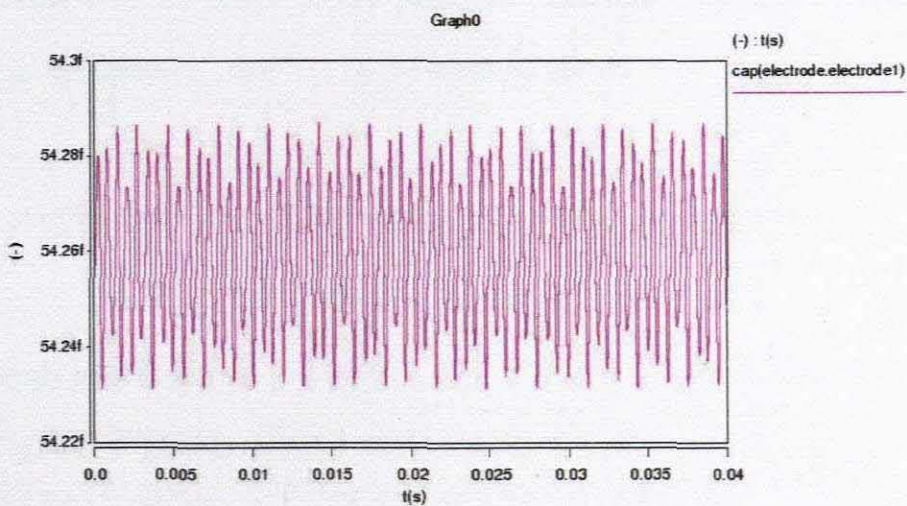
Figure 4.25: Transient Analysis of Capacitance

4.3.7 Impact of Plate Curvature Analysis

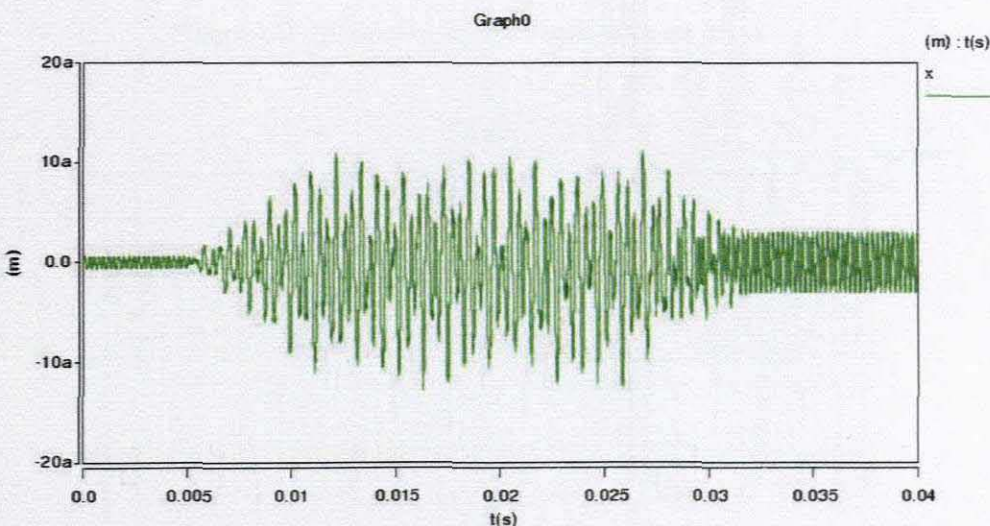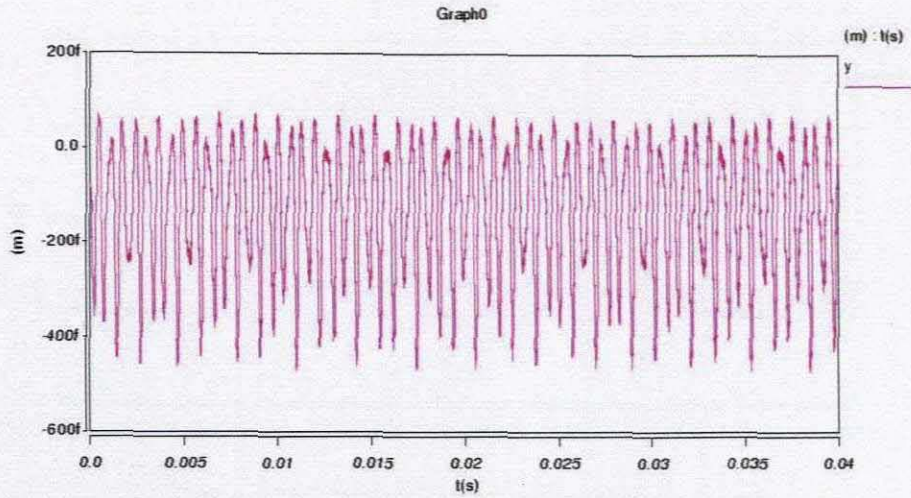MEMS structures are typically deformed by surface stress caused by the manufacturing process. The common curvature parameter can be used to study the impact of rigid plate curvature on the device performance. The curvature parameter is available in the rigid plate, beam, and the electrode components.

With the six sub-parameters of the component parameters (x_0, y_0, c_1, c_2, c_3, c_4, c_5), we can specify a parabolic curvature surface of a rigid plate in the reference coordinate system:

$$z = f(x,y) = c_1(x-x_0)^2 + c_2(y-y_0)^2 + c_3(x-x_0)(y-y_0) + c_4(x-x_0) + c_5(y-y_0)$$

The constants of curvature profile are usually derived from interferometric measurements of the released structure or by measuring the vertical position of designated points such as plate corners or the plate center. Alternatively, if the material stress gradients of the fabrication process are well known, plate bending can be analyzed in a FEM verification step using MemMech of CoventorWare.

In this simulation we assume a symmetric bending of the perforated plate with its local minimum in the center of the plate. We therefore only need to specify the polynomial constants c_1, and c_2 of the equation above.

We will start by specifying a fixed curvature by setting the design variable to $c_1 = 1$ and $c_2 = 1$. The simulated parabolic curvature surface of a rigid plate will consequently be set to:

$$z = f(x,y) = x^2 + y^2$$

The corners of the plate will consequently experience a vertical displacement of $320nm$.
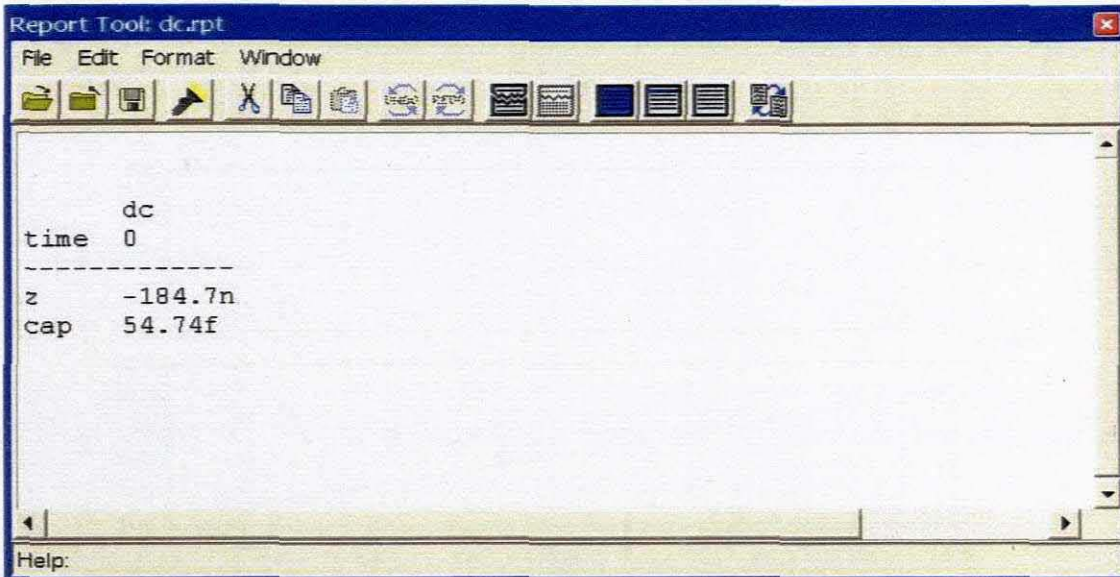
Figure 4.26: DC operating point report for curvature plate

The applied curvature causes a central knot to move $184.7nm$ (Figure 4.26) in negative z direction, which is about $180nm$ below the initial equilibrium without curvature. The new equilibrium is mainly the result of the curvature-caused offset of the beam-ends that are connected to the plate.

The second pin, cap, shows the curvature-caused capacitance between the detection electrode and the curved plate. The apparently tiny curvature is causing a capacitance reduction of about 0.92%, which will make a important effect on the sensitivity of the device.

Fabrication defects like plate curvature and beam sidewall angles are often causing of mismatches between measured and simulated data. Furthermore, unsymmetrical plate curvature (mismatch between the plate center and the local minimum x_0, y_0 of the assumed parabolic shape) are often the source of unexpected device behavior like staggering motions and an increased cross sensitivity.

In this project, we assume the curvature coefficient c_1 and c_2 form 0.4 to 2, and Figure 4.27 gives us the impact for displacement on z direction and capacitance.
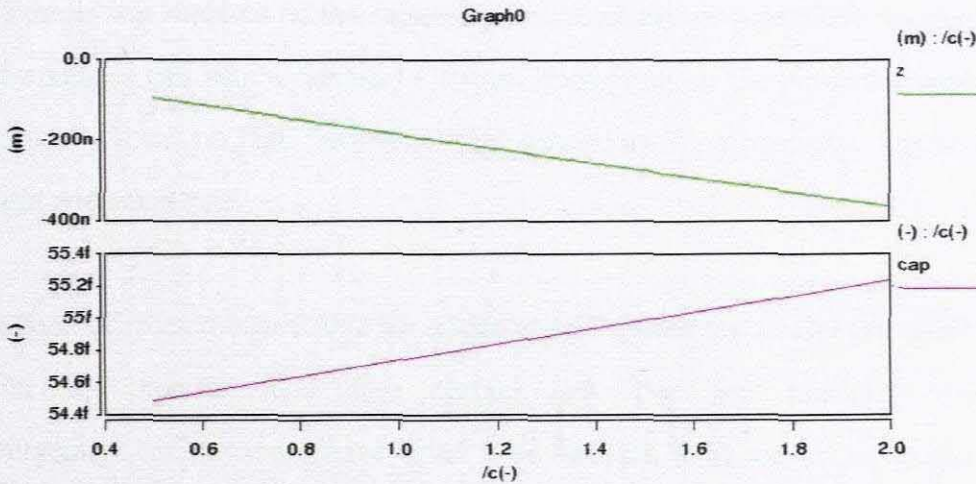
Figure 4.27: Result of the vary analysis

Figure 4.26 tells us, that for this device, the curvature effect on the first resonance frequencies is very small.

4.4   Summary

In this chapter, the analytical model for bridge-type capacitive micro accelerometer has been analyzed. The properties of the accelerometer have been impressed on formulation.

In the first part of this chapter, the analytical model was analyzed on Energy Method. The formulas of the characteristics have been calculated. Then the imaginary model is analyzed according these formulas. In the second part of this chapter, the imaginary model was analyzed with CoventorWare 2004. All the results prove the analytical formulas of the analytical model are right.

Chapter 5

Conclusions and Recommendations

5.1   Summary

This thesis was directed on the capability studies of bridge-type micro accelerometer. Performances can take a number of forms, depending on the particular application, but usually focus on high frequency, high sensitivity, high precision, low cost, light weight and small size.

The general accelerometers that have been manufactured previously can only provide ecumenical precision and have normal size. The high precision and large impingement measurement have never been realized until the micro accelerometer have been studied and manufactured. Up to now, micro accelerometer has been used in many applications on different field, such as aerospace structures, MEMS and other high-tech industry. In line with the improvement of applications, the micro accelerometer with different types and structures has been requested for providing more accurate measurement. This thesis was motivated by this challenge.

The piezoelectric accelerometer and capacitive accelerometer have been become more and more popular in micromation-transducer field. The major goal of this work was to gain some guidelines of the piezoelectric thin films read-out and capacitive accelerometers with bridge-type suspending beam at first. Secondly, the two connecting configures of bridge-type micro accelerometer with two piezoelectric thin films read-out have been compared in this work. The following objectives have been done in this work:

- Study the analytical models for bridge-type micro accelerometers with two piezoelectric thin films read-out

- Compare the two connecting configurations of bridge-type micro accelerometers with two piezoelectric thin films read-out

- Study the analytical models for bridge-type capacitive micro accelerometers

The first objective and the second objective were investigated in Chapter 3 at the same time. This chapter dealt with the analysis of the bridge-type micro accelerometers with two piezoelectric thin films read-out which have two connecting configures. All of the main characters of these two configures have been calculated, such as accelerometer formula, sensitivity, noise, minimum detectable signal (MDS), resonance frequency and maximum detectable range.

The third objective was solved in Chapter 4. In this chapter, except analysis of the model, CoventorWare was used to analyze the proposed model. The characteristics of bridge-type capacitive micro acceleration have been discussed by the analytical and numerical results.

5.2   Conclusions

In this work, the capability of the two types of accelerometer has been studied. And the two connecting configures of the bridge-type micro accelerometers with two piezoelectric thin films read-out have been discussed for the further applications.

Comparing the two types of accelerometers, the maximum detectable range of bridge-type micro accelerometers with two piezoelectric thin films read-out is much more than bridge-type capacitive micro accelerometer. And because the bridge-type micro accelerometers with two piezoelectric thin films read-out is an incorporate structure, its size is smaller than capacitive accelerometer. So the bridge-type micro accelerometers with two piezoelectric thin films read-out is more fit on the large acceleration, tiny size condition. However, the sensitivity of bridge-type capacitive

micro accelerometer is higher than that of bridge-type micro accelerometers with two piezoelectric thin films read-out. Therefore, the bridge-type capacitive micro accelerometer can be used in the high sensitive measurement.

Analysis of Bridge-Type Micro Accelerometers with Two Piezoelectric Thin Films Read-Out

The analysis of bridge-type micro accelerometers with two piezoelectric thin films read-out has been done in Chapter 3. The formulas for main parameters have been listed in Table 5.1.

Table 5.1: Properties formula of accelerometer

	Piezoelectric Accelerometer in Serial Configure	Piezoelectric Accelerometer in Parallel Configure	Capacitive Accelerometer
Accelerometer Formula	$Q_s = 0.12375 d_{31} b \dfrac{E_p}{EI_{eq}} \left(\dfrac{h_{pzt}}{2} + a \right) l^2 m \ddot{z}$	$Q_p = 0.125 d_{31} b \dfrac{E_p}{EI_{eq}} \left(\dfrac{h_{pzt}}{2} + a \right) l^2 m \ddot{z}$	$\Delta C = \dfrac{m l^2 \varepsilon_0 s}{2 E b h^3 \delta_0^2} \ddot{z}$
Resonance Frequency	$f = \dfrac{1}{2\pi} \sqrt{\dfrac{2 E I_{eq}}{m l^3}}$		$f = \dfrac{1}{2\pi} \sqrt{\dfrac{2 E b h^3}{m l^3}}$
Bandwidth	$BW = \dfrac{\sqrt{k/m}}{Q}$		
Sensitivity	$S_v^s = 0.12375 d_{31} b \dfrac{E_p}{EI_{eq}} \left(\dfrac{h_{pzt}}{2} + a \right) \dfrac{l^2 m}{C_s}$	$S_v^p = 0.125 d_{31} b \dfrac{E_p}{EI_{eq}} \left(\dfrac{h_{pzt}}{2} + a \right) \dfrac{l^2 m}{C_p}$	$S_{v1} = \dfrac{\Delta C}{\Delta \delta} = \dfrac{\varepsilon_0 s}{\delta_0^2}$ $S_{v2} = \dfrac{\Delta C}{\ddot{z}} = \dfrac{m l^2 \varepsilon_0 s}{2 E b h^3 \delta_0^2}$
Quality Factor	$Q = \dfrac{d \sqrt{mk}}{\mu_0 A}$		
Brown Noise Equivalent Acceleration	$a_\varepsilon = \sqrt{\dfrac{4 k_B T \mu_0 A}{d m^2}}$		
MDS	$MDS = \dfrac{\mu_0 A}{d} \times \sqrt{\dfrac{4 k_B T}{m^3}}$		
Maximum Detectable Range	$\ddot{z}_{max} = \dfrac{4 \sigma_r E I_{eq}}{E_p m l (h - a)}$		$\ddot{z}_{max} = \dfrac{4 b h^3 (1 - \mu^2) \sigma_{max}}{3 m l^2}$

Comparing Two Connecting Configures of Bridge-Type Micro Accelerometers with Two Piezoelectric Thin Films Read-Out

To one group piezoelectric transducer, there are two connecting configures for this type of accelerometer. The main parameters of those configures in shown in Table 5.1. In Chapter 3, the difference between the two connecting configures of bridge-type micro accelerometers with two piezoelectric thin films read-out have been discussed. Compare to parallel configure, the serial configure can provide more than 4 times sensitivity with almost same output charge. It means, bridge-type micro accelerometers with two piezoelectric thin films read-out in serial configure have more accurate output data and more sensitive response with the same acceleration which is detected.

Analysis of Bridge-Type Capacitive Micro Accelerometer

As a very popular transducer, bridge-type capacitive micro accelerometer was studied in Chapter 4. The analytical formulas are also shown in Table 5.1. On the base of it, CoventorWare was used to analyze the model. Through those result, the impact of the dimension and tolerance was expressed. It will be very important warrant in design.

5.3   Recommendations for Future Work

Now, the analysis of two types of bridge-type micro accelerometers has completed. Through calculating and simulating the models, the mechanical performances can be forecasted before building the prototypes. In this work, the electrical static force does not be considered when bridge-type capacitive accelerometer was analyzed, so there will be some error in the formulas.

The future work will be focused on some directions of new structure designing and application in industry field. First direction is about the new structure designing to increase the resonance frequency and sensitivity. Then the transducer can be used to detect larger acceleration and smaller mass. Second research direction is about complex function transducer. Due to the requirement of industry field, especially the aerospace, the incorporate complex function transducer, such as incorporate gyroscope, becomes a development trend. It will make the fabricating cost of

transducers reduce, and can leave more space to locate other devices. Micro intelligentized transducers will be the third direction. Along with the subminiature robot development, the micro intelligentized transducers beget the attention of the academician. The micro intelligentized transducers can make the robot easier to control, more agility, and more clever.

Bibliography

[Boser, 1996] B. Boser and R. T. Howe, 1996, Surface micromachined accelerometers, IEEE J. Solid-State Circuits, vol. 31, p. 366–375

[Chau, 1995] K. Chau, S. R. Lewis, Y. Zhao, R. T. Howe, S. F. Bart, and R. G. Marcheselli, 1995, An integrated force-balanced capacitive accelerometer for low-g applications, in Tech. Dig. 8th Int. Conf. on Solid-State Sensors and Actuators (Transducers'95), Stockholm, Sweden, p. 593–596

[Cole, 1991] J. C. Cole, 1991, A new sense element technology for accelerometer subsystems, in Tech. Dig. 6th Int. Conf. Solid-State Sensors and Actuators (Transducers'91), San Francisco, CA, p. 93–96

[Connor, 1982] F. R. Connor, 1982, Noise, Second Edition, ISBN 0 7131 3459 3

[Coulon, 1993] Y. de Coulon, T. Smith, J. Hermann, M. Chevroulet, and F. Rudolf, 1993, Design and test of a precision servoaccelerometer with digital output, in Tech. Dig. 7th Int. Conf. Solid-State Sensors & Actuators (Transducers'93), p. 832–835

[Drieenhuizen, 1997] B. P. van Drieenhuizen, N. Maluf, I. E. Opris, and G. Kovacs, 1997, Force-balanced accelerometer with mG resolution fabricated using silicon fusion bonding and deep reactive ion etching, in Tech. Dig. 9th Int. Conf. Solid-State Sensors and Actuators (Transducers'97), Chicago, IL, p. 1229–1230

[Gabrielson, 1993] T. B. Gabrielson, 1993, Mechanical-thermal noise in micromachined acoustic and vibration sensors, IEEE Trans, Electron. Devices, Vol. 40:903-909

[Henrion, 1990] W. Henrion, L. DiSanza, M. Ip, S. Terry, and H. Jerman, 1990, Wide-dynamic range direct digital accelerometer, in Tech. Dig. Solid-State Sensors and Actuators Workshop, Hilton Head Island, SC, p. 153–156

[Hordeski, 1985] M. F. Hordeski, 1985, Microprocessor sensor & control systems, p. 334-345

[Http, a] http://www.mmf.de

[Http, b] http://www.pc-control.co.uk

[Http, c] http://xenia.media.mit.edu/~verp/projects/smartpen/node17.html

[Ma, 1994] K. J. Ma, N. Yazdi, and K. Najafi, 1994, A bulk-silicon capacitive microaccelerometer with built-in overrange and force feedback electrodes, in Tech. Dig. Solid-State Sensors and Actuators Workshop, Hilton Head Island, SC, p. 160–163

[McCallion, 1973] H. McCallion, 1973, Vibration of Linear Mechanical Systems, Longman Group, London, p.103

[Norton, 1982] Harry N. Norton, 1982, Sensor and analyzer handbook, pp. 64-69

[Peeters, 1992] E. Peeters, S. Vergote, B. Puers, and W. Sansen, 1992, A highly symmetrical capacitive micro-accelerometer with single degreeof-freedom response, J. Micromech. Microeng., vol. 2, p. 104–112

[Petersen, 1982] K. Petersen, 1982, Silicon as a mechanical material, Proc. IEEE, Vol.70

[Ristic, 1993] L. Ristic, R. Gutteridge, J. Kung, D. Koury, B. Dunn, and H. Zunino, 1993, A capacitive type accelerometer with self-test feature based on a double-pinned polysilicon structure, in Tech. Dig. 7th Int. Conf. Solid-State Sensors and Actuators (Transducers'93), p. 810–812

[Rocksatd, 1995] H. K. Rocksatd, J. K. Reynolds, T. K. Tang, T. W. Kenny, W. J. Kaiser, and T. B. Gabrielson, 1995, A miniature, high-sensitivity, electron-tunneling accelerometer, in Tech. Dig. 8th Int. Conf. Solid-State Sensors and Actuators (Transducers'95), Stockholm, Sweden, p. 675–678

[Rudolf, 1987] F. Rudolf, A. Jornod, and P. Bencze, 1987, Silicon microaccelerometers, in Tech. Dig. 4th Int. Conf. Solid-State Sensors and Actuators (Transducers'87), p. 376–379

[Rudolf, 1990] F. Rudolf, A. Jornod, J. Berqovist, and H. Leuthold, 1990, Precision accelerometers with g resolution, Sensors Actuators, vol. A21/A23, p. 297–302

[Seidel, 1990] H. Seidel, R. Reidel, R. Kolbeck, G. Muck, W. Kupke, and M. Koniger, 1990, Capacitive silicon accelerometer with highly symmetric design, Sensors Actuators, vol. A21/A23, p. 312–315

[Selvakumar, 1996] A. Selvakumar, F. Ayazi, and K. Najafi, 1996, A high sensitivity -axis torsional silicon accelerometer, in Tech. Dig. IEEE Int. Electron Device Meeting, San Francisco, CA, p. 765–768

[Selvakumar, 1997] A. Selvakumar, 1997, A multifunctional silicon micromachining technology for high performance microsensors and microactuators, Ph.D. dissertation, University of Michigan, Ann Arbor

[Sherman, 1992] S. J. Sherman, W. K. Tsang, T. A. Core, R. S. Payne, D. E. Quinn, K. H. Chau, J. A. Farash, and S. K. Baum, 1992, A low-cost monolithic accelerometer: Product/technology update, in Tech. Dig. IEEE Electron Devices Meeting (IEDM'92), p. 160–161

[Smith, 1994] T. Smith, O. Nys, M. Chevroulet, Y. DeCoulon, and M. Degrauwe, 1994, A 15b electromechanical sigma–delta converter for acceleration measurements, in Tech. Dig. IEEE Int. Solid-State Circuits Conf. (ISSCC'94), San Francisco, CA, p. 160–161

[Spangler, 1995] L. Spangler and C. J. Kemp, 1995, ISAAC–Integrated silicon automotive accelerometer, in Tech. Dig. 8th Int. Conf. Solid-State Sensors and Actuators (Transducers'95), Stockholm, Sweden, p. 585–588

[Sun, 2004] B. H. Sun, and R. Zhang, 2004, MEMS sccelerometer with two thin film piezoelectric read-out, Journal of Ningbo University, Vol.17 Sup (2004), p.71-75

[Sun, 2005] B. H. Sun, and R. Zhang, 2005, MEMS pressure sensor with two thin film piezoelectric read-out, Proceedings of Nanotech2005, Anaheim, California, p.624-627

[Wang, 2004] Qing-Ming Wang, Zhaochun Yang, Fang Li, Patrick Smolinski, 2004, Analysis of thin film piezoelectric microaccelerometer using analytical and finite element modeling, Sensor and Actuators A 113 (2004)1-11

[Warren, 1994] K. Warren, 1994, Navigation grade silicon accelerometer with sacrificially etched SIMOX and BESOI structure, in Tech. Dig. Solid-State Sensors and Actuators Workshop, Hilton Head Island, SC, p. 69–72

[Yazdi, 1977] N. Yazdi and K. Najafi, 1977, An all-silicon single-wafer fabrication technology for precision microaccelerometers, in Tech. Dig. 9th Int. Conf. Solid-State Sensors and Actuators (Transducers'97), Chicago, IL, p. 1181–1184

[Yeh, 1995] C. Yeh and K. Najafi, 1995, A low-voltage bulk-silicon tunnelingbased microaccelerometer, in Tech. Dig. IEEE Int. Electron Devices Meeting (IEDM), Washington, DC, p. 593–596

[Yu, 2001] J. C. Yu, and C. B. Lan, 2001, System modeling of microaccelerometer using piezoelectric thin films, Sensors and Actuators A, 88: 178–186

Appendix A

Introduction of CoventorWare 2004

CoventorWare is the most comprehensive suite of MEMS design tools in the industry. It acts as a seamless integrated design environment that reduces design risk, speeds time-to-market and lowers development costs.

CoventorWare supports both system-level and physical approaches to designing MEMS and micro fluidic devices. The system-level approach involves use of behavioral model libraries with a high-speed system simulator. The system-level design can be used to generate a 2-D layout for physical level verification. The physical approach starts with a 2-D layout and involves building a 3-D model, generating a mesh, and simulating using FEM or BEM solvers. Custom reduced-order macromodels can be extracted for use in system simulations. Finally, the verified 2-D layout can be transferred to a foundry for fabrication. CoventorWare has numerous options, including design libraries and a variety of 3-D physics solvers. Various entry and exit points allow import and export of files from and to other third-party software, for example, the software by the name of MATLAB and Solid Works etc.

CoventorWare can be described as a circularly connected series of modules. Designs may begin at different places in this flow, depending on whether users choose to design at the system or physical level.

Figure Appendix A.1 is a flow map which can show us how this software works.
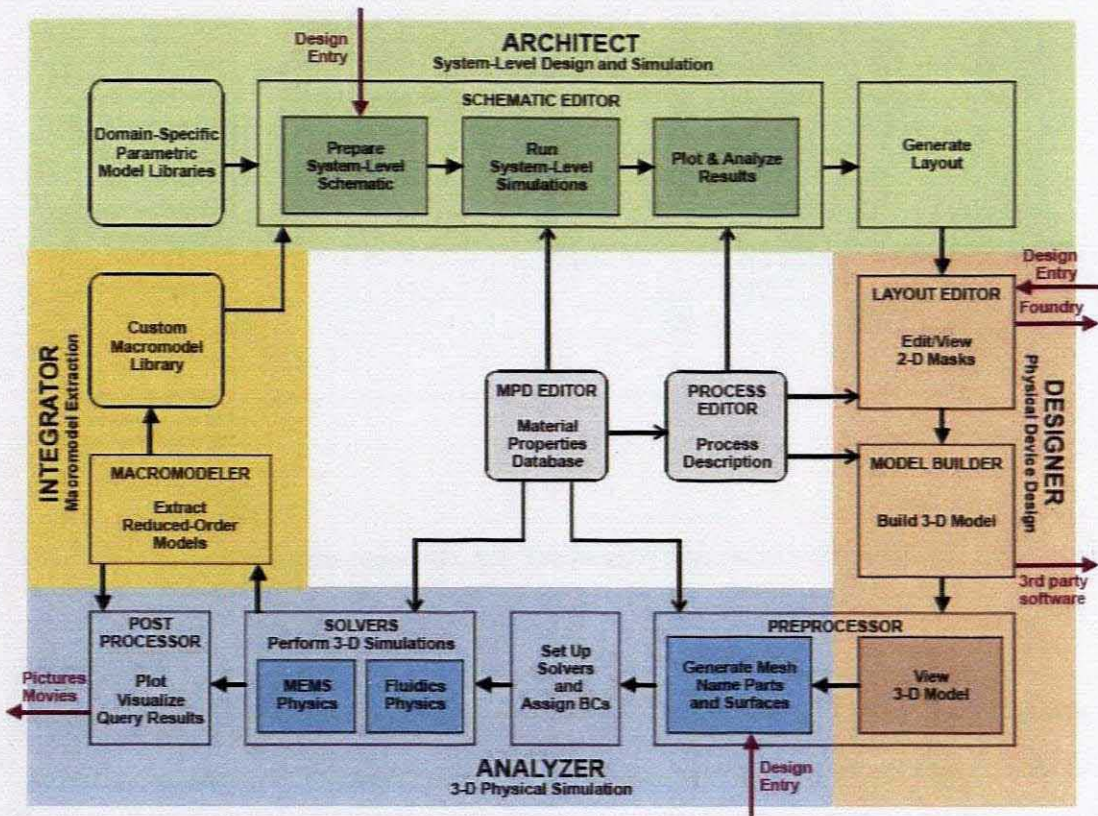
Figure Appendix A.1: The flow map of CoventorWare working

CoventorWare products are available separately or bundled in various configurations to conform to the customer's preferred design flow, methodology and application. CoventorWare consists of four main modules that may be used stand-alone or integrated into a complete design flow:

ARCHITECT:

ARCHITECT offers a rich set of parameterized expanded MEMS component libraries, a schematic capture engine, and a proven, fully capable simulation engine. Individual libraries support a wide variety of MEMS and microfluidics applications, including electromechanical, RF, fluidic, magnetic, and optical, as well as the specialized physics required for these applications. Customize components by inputting geometry and material property information, then combine them in a schematic layout to create an accurate models of a MEMS device. Run accurate simulations on models up to 100 times faster than with equivalent 3-D numerical models. The block diagram (Figure Appendix A.2) outlines the steps. The shaded boxes represent architect functionality.
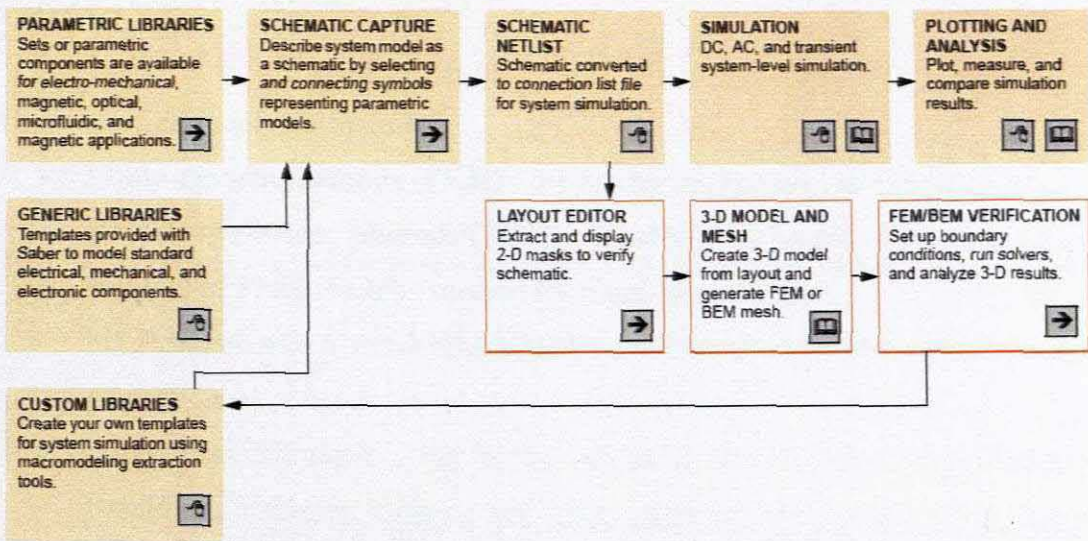
Figure Appendix A.2: The block diagram of architect work

DESIGNER:

DESIGNER consists of three functional building blocks: a 2D GDSII layout editor, a geometry editor and material property database, and a 3D preprocessor. The fully capable 2D GDSII layout editor supports a variety of import and export formats. The geometry editor and material property database, which ARCHITECT and ANALYZER can use and update, serves as a repository for all of the information necessary for building manufacturing processes for a device. The 3D model preprocessor comes with a tree and canvas GUI.

Use DESIGNER standalone, with ARCHICTECT and/or ANALYZER, or with third-party tools. With ARCHITECT, use DESIGNER to specify detailed geometry and material information necessary to automatically configure ARCHITECT parameterized models. DESIGNER also supports schematic-driven layout capabilities that automatically generate GDSII layout information from the optimized MEMS schematic model. When used with ANALYZER, DESIGNER pre-processes models directly. DESIGNER outputs the industry-standard SAT 3D geometry format supported by most third-party field solver products.

ANALYZER:

ANALYZER is a multi-physics numerical analysis framework. Customers may customize ANALYZER by choosing field solvers that address the physics necessary

for mechanical, electrical, thermal, electromagnetic, microfluidic, and optical analysis.

The best-of-class solvers include:
- **Finite element methods (FEM)** - for mechanics and general fluidics
- **Boundary element methods (BEM)** - for electrostatics and inductance
- **Volume of Fluid (VOF)** - method for multi-phase fluidics
- **3D Preprocessor** - All ANALYZER bundles include MEMS-specific mesh generation.
- **Simulation Manager** - for seting up field solvers, managing boundary conditions, initiating solution sequences, and capturing and storing design data.
- **Visualization Post Processor** - for analyzing solver resuts and creating 2D and 3D graphical output

INTEGRATOR:
INTEGRATOR creates non-linear complex reduced-order MEMS models from detailed models created in ANALYZER that run in system simulation tools. Analyze in and/or export these models to industry-standard IC simulators from Synopys and Cadence, or reuse the results in Matlab-Simulink

INTEGRATOR reduces the detailed 3D analysis produced in ANALYZER into a reduced-order model that fully characterizes the behavior of the device using a small number of parameters (six degrees of displacement and five degrees of electrical freedom). INTEGRATOR can then export these reduced order models in formats that support Synopsys, Cadence, and MatLab for inclusion in integrated circuit designs.

Appendix B

Constitution of Piezoelectric Accelerometer with Piezoelectric Thin Film Read Out

To fabricate a virtual model of a device in CoventorWare, the material properties must be defined in MPD first, Figure Appendix B.1-B.5 show the properties of the material used in this work:
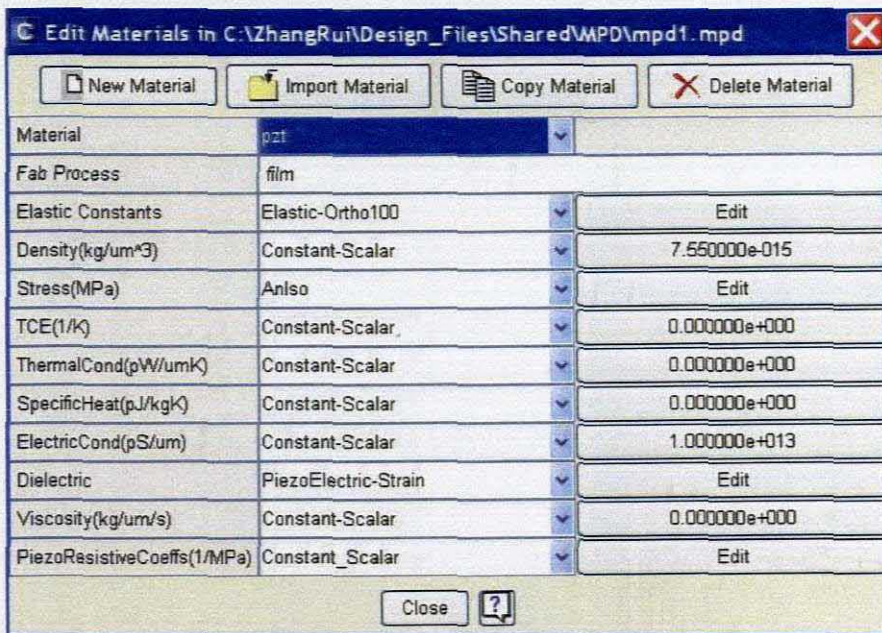

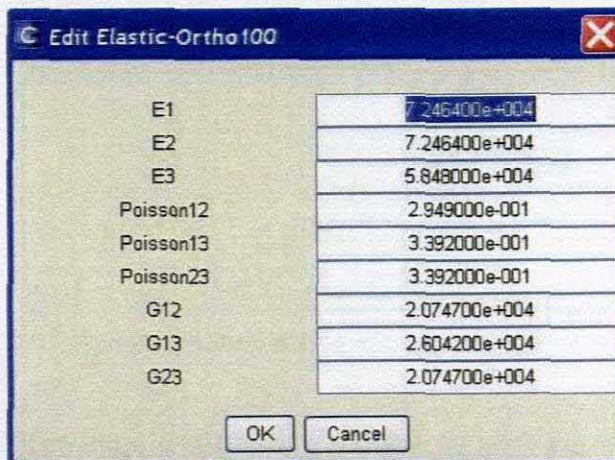**Figure Appendix B.1**: material properties of piezoelectric thin film

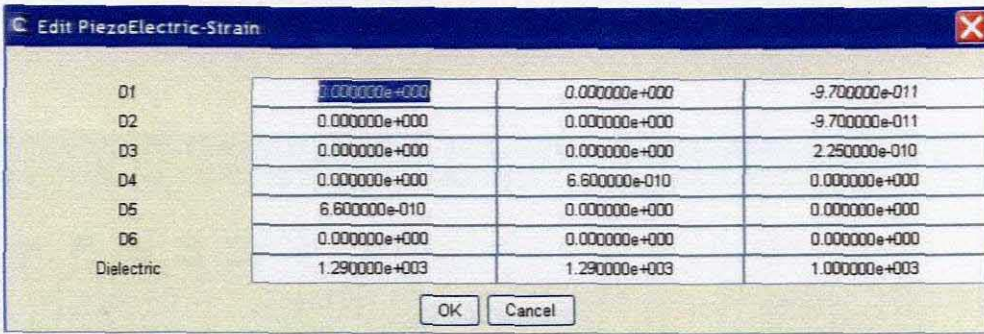**Figure Appendix B.2**: elastic constants of piezoelectric thin film

D1	0.000000e+000	0.000000e+000	-9.700000e-011
D2	0.000000e+000	0.000000e+000	-9.700000e-011
D3	0.000000e+000	0.000000e+000	2.250000e-010
D4	0.000000e+000	6.600000e-010	0.000000e+000
D5	6.600000e-010	0.000000e+000	0.000000e+000
D6	0.000000e+000	0.000000e+000	0.000000e+000
Dielectric	1.290000e+003	1.290000e+003	1.000000e+003

Figure Appendix B.3: dielectric constants of piezoelectric thin film

Edit Materials in C:\ZhangRui\Design_Files\Shared\MPD\mpd1.mpd

New Material Import Material Copy Material Delete Material

Material	Silicon	
Fab Process	FILM	
Elastic Constants	Elastic-Iso	Edit
Density(kg/um^3)	Constant-Scalar	2.330000e-015
Stress(MPa)	AnIso	Edit
TCE(1/K)	Constant-Scalar	2.500000e-006
ThermalCond(pW/umK)	Constant-Scalar	1.480000e+008
SpecificHeat(pJ/kgK)	Constant-Scalar	7.120000e+014
ElectricCond(pS/um)	Constant-Scalar	0.000000e+000
Dielectric	Constant-Scalar	7.300000e+002
Viscosity(kg/um/s)	Constant-Scalar	0.000000e+000
PiezoResistiveCoeffs(1/MPa)	Constant_Scalar	Edit

Close

Figure Appendix B.4: material properties of silicon

Edit Elastic-Iso

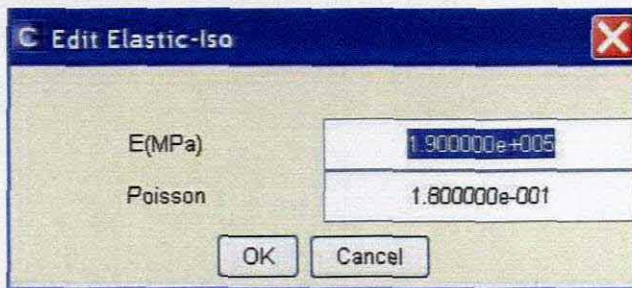|	
E(MPa)	1.900000e+005
Poisson	1.600000e-001

OK Cancel

Figure Appendix B.5: Elastic constants of silicon

ProcessEditor describes the manufacturing process and defines the thickness of each layer. Therefore, the devices can be fabricated following these steps. Figure Appendix

B.6 gives the process of the bridge-type capacitive micro accelerometer performed in this thesis.

Step	Action	Type	Layer Name	Material	Thickness	Color	Polarity	Depth	Offset	Sidewall Angle	Cor
0	Base		Substrate	SILICON	50.0	white	GND				
1	Deposit	Planar	Sacrifice	BPSG	295.0	yellow					
2	Etch	Front, Last L..				yellow	Sacrifice -	295.0	0.0	0.0	
3	Deposit	Planar	mass	Silicon	5.0	cyan					
4	Etch	Front, Last L..				cyan	mass +	5.0	0.0	0.0	
5	Deposit	Planar	beam	Silicon	0.0	blue					
6	Etch	Front, Last L..				blue	beam +	5.0	0.0	0.0	
7	Deposit	Planar	pzt	pzt	0.5	orange					
8	Etch	Front, Last L..				orange	pzt +	0.5	0.0	0.0	

Figure Appendix B.6: Manufacturing process of piezoelectric accelerometer

2-D layout must be drawn manually as Figure Appendix B.7 and be complied the layer definitions in ProccessEditor.
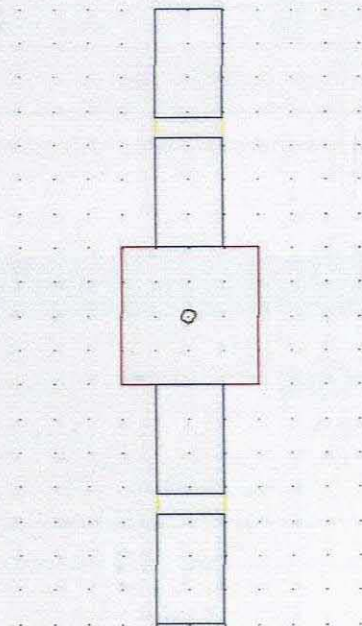

Figure Appendix B.7: 2-D layout for piezoelectric accelerometer

Then the 3-D model can be created automatically.

Appendix C
Constitution of Capacitive Accelerometer

The properties of silicon are defined as Figure Appendix B.4 and B.5. The properties of aluminum are shown on Figure Appendix C.1 and C.2:
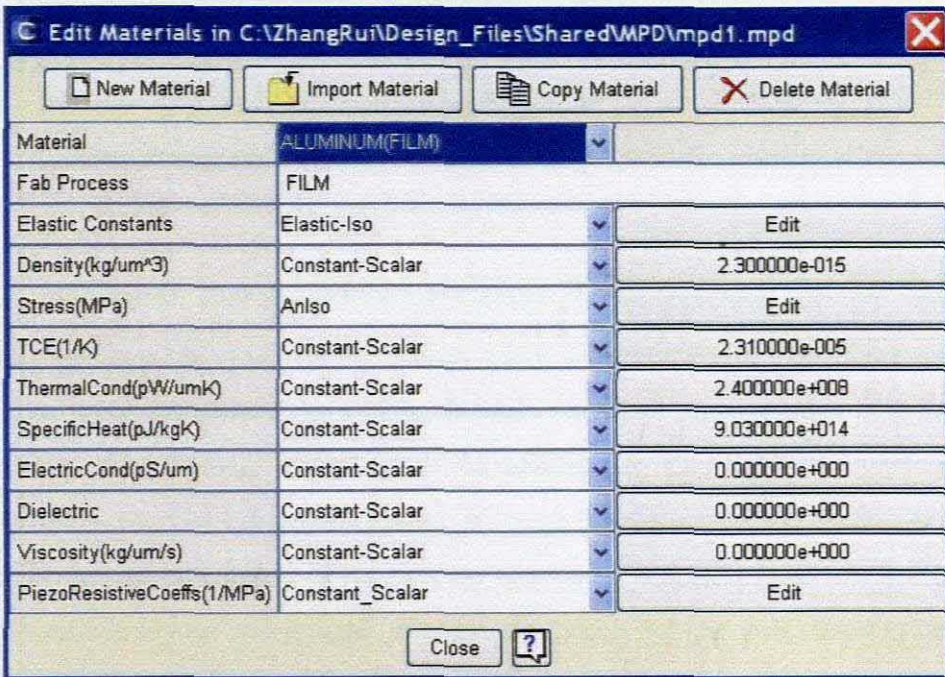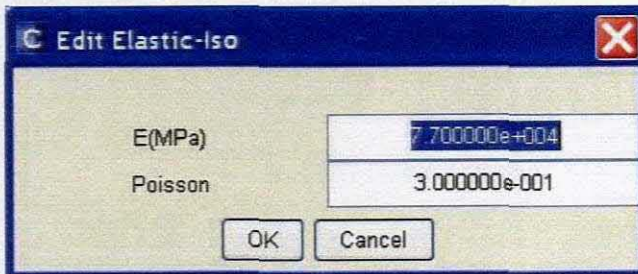
C Edit Materials in C:\ZhangRui\Design_Files\Shared\MPD\mpd1.mpd			
New Material	Import Material	Copy Material	Delete Material
Material	ALUMINUM(FILM)		
Fab Process	FILM		
Elastic Constants	Elastic-Iso		Edit
Density(kg/um^3)	Constant-Scalar		2.300000e-015
Stress(MPa)	Anlso		Edit
TCE(1/K)	Constant-Scalar		2.310000e-005
ThermalCond(pW/umK)	Constant-Scalar		2.400000e+008
SpecificHeat(pJ/kgK)	Constant-Scalar		9.030000e+014
ElectricCond(pS/um)	Constant-Scalar		0.000000e+000
Dielectric	Constant-Scalar		0.000000e+000
Viscosity(kg/um/s)	Constant-Scalar		0.000000e+000
PiezoResistiveCoeffs(1/MPa)	Constant_Scalar		Edit
Close ?			

Figure Appendix C.1: material properties of aluminum

C Edit Elastic-Iso	
E(MPa)	7.700000e+004
Poisson	3.000000e-001
OK	Cancel

Figure Appendix C.2: elastic constants of aluminum

Manufacturing process is like Figure Appendix C.3.

Figure Appendix C.3: Manufacturing process of capacitive accelerometer

The Parametric Electromechanical Library is an essential design resource for electromechanical system-level design using CoventorWare. The library consists of system level components available through Architect and includes both mechanical and electromechanical components. In addition to the ability to perform system simulation, the EM Library Reference is constructed to enable automatic extraction of the layout and generation of the process sequence. A solid model file is created from the available layout and process information, and is subsequently used in device level simulation for validation and optimization.
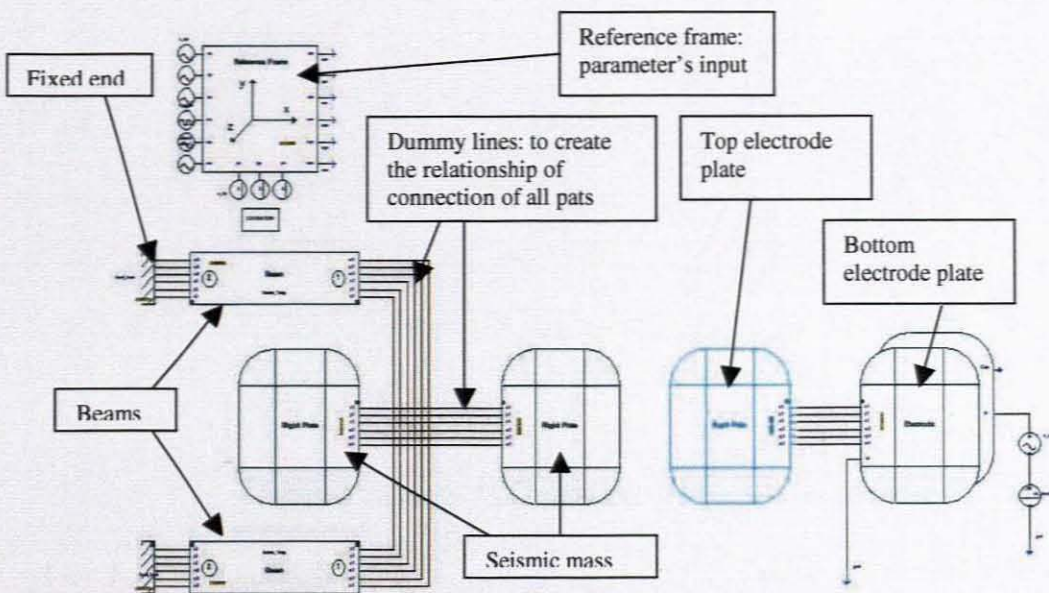

Figure Appendix C.4: Architect model for capacitive accelerometer
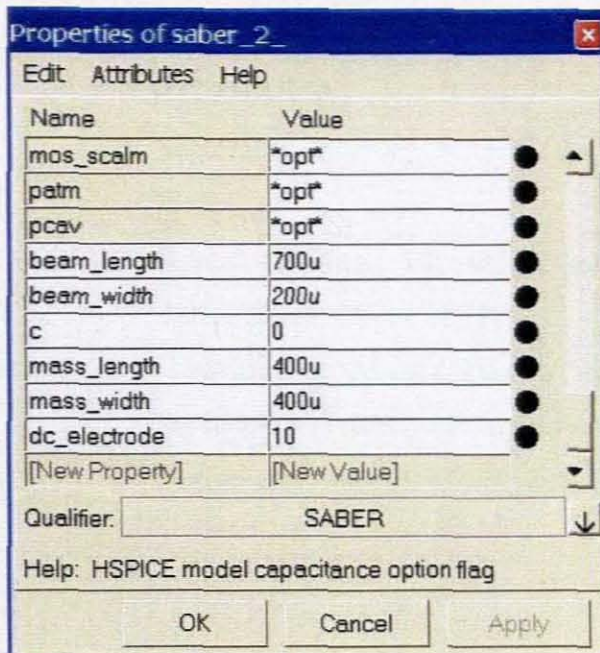
Figure Appendix C.5: the parameter of the device

The 2-D layout can be created automatically as Figure Appendix C.6 complied with Parametric Electromechanical Library. And integrating the processor and 2-D layout, 3-D model can be obtained.
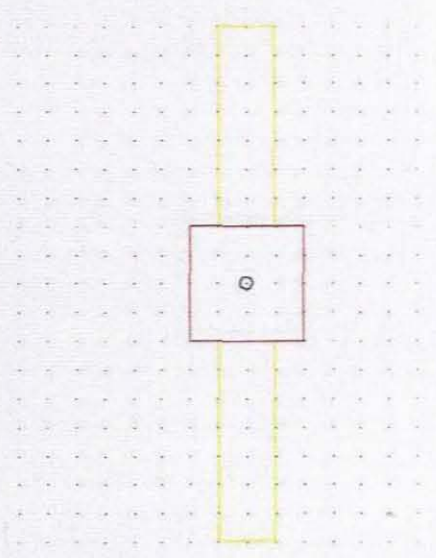

Figure Appendix C.6: 2-D layout of capacitive accelerometer

Resume of Rui ZHANG

Name: Rui ZHANG

Birth: September 26, 1981

Gender: Male

Degree: B.Sc. (Beijing University of Aeronautics and Astronautics, China, 2002)

Current Situation: Studying for Master Degree of Technology (Cape Peninsula University of Technology, South Africa)

Research Interests: Design and Analysis of Micro Accelerometers

Publication:

Journal Paper:

Bohua Sun, and Rui Zhang, 2004, MEMS sccelerometer with two thin film piezoelectric read-out, Journal of Ningbo University, Vol.17 Sup (2004), p.71-75

Conference Paper:

Bohua Sun, and Rui Zhang, 2005, MEMS pressure sensor with two thin film piezoelectric read-out, Proceedings of Nanotech2005, Anaheim, California, p.624-627